2019

DETERMINING RATES OF LANDSCAPE RESPONSE TO TECTONIC FORCING ACROSS A RANGE OF TEMPORAL SCALES AND EROSIONAL MECHANISMS: TETON RANGE, WY

Meredith Swallom
University of Kentucky, meredith.swallom@gmail.com
Digital Object Identifier: https://doi.org/10.13023/etd.2019.310

STUDENT AGREEMENT:

I represent that my thesis or dissertation and abstract are my original work. Proper attribution has been given to all outside sources. I understand that I am solely responsible for obtaining any needed copyright permissions. I have obtained needed written permission statement(s) from the owner(s) of each third-party copyrighted matter to be included in my work, allowing electronic distribution (if such use is not permitted by the fair use doctrine) which will be submitted to UKnowledge as Additional File.

I hereby grant to The University of Kentucky and its agents the irrevocable, non-exclusive, and royalty-free license to archive and make accessible my work in whole or in part in all forms of media, now or hereafter known. I agree that the document mentioned above may be made available immediately for worldwide access unless an embargo applies.

I retain all other ownership rights to the copyright of my work. I also retain the right to use in future works (such as articles or books) all or part of my work. I understand that I am free to register the copyright to my work.

REVIEW, APPROVAL AND ACCEPTANCE

The document mentioned above has been reviewed and accepted by the student's advisor, on behalf of the advisory committee, and by the Director of Graduate Studies (DGS), on behalf of the program; we verify that this is the final, approved version of the student's thesis including all changes required by the advisory committee. The undersigned agree to abide by the statements above.

Meredith Swallom, Student

Dr. J. Ryan Thigpen, Major Professor

Dr. Ed Woolery, Director of Graduate Studies

DETERMINING RATES OF LANDSCAPE RESPONSE TO TECTONIC FORCING ACROSS A RANGE OF TEMPORAL SCALES AND EROSIONAL MECHANISMS: TETON RANGE, WY

THESIS

A thesis submitted in partial fulfillment of the
requirements for the degree of Master of Science in the
College of Arts and Sciences
at the University of Kentucky

By

Meredith Leigh Swallom

Lexington, Kentucky

Director: Dr. J. Ryan Thigpen, Professor of Earth and Environmental Sciences

Lexington, Kentucky

2019

ABSTRACT OF THESIS

DETERMINING RATES OF LANDSCAPE RESPONSE TO TECTONIC FORCING ACROSS A RANGE OF TEMPORAL SCALES AND EROSIONAL MECHANISMS: TETON RANGE, WY

Understanding how mountain landscapes respond to variations in tectonic forcing over a range of temporal scales in active mountain belts remains as a prominent challenge in tectonic and geomorphological studies. Although a number of empirical and numerical studies have examined this problem, many of them were complicated by issues of scale and climatic variability. More specifically, the relative efficiencies of fluvial and glacial erosion, which are presumably controlled by climate, are difficult to unravel. The Teton Range in Wyoming, which results from motion on the crustal-scale Teton fault, is an ideal natural laboratory for addressing this challenge as the tectonic uplift boundary condition and the variation of uplift along strike is well-documented by previous studies and due to its relatively small size, climate can be reasonably expected to vary consistently along strike. Here, we present the results from a study that examines how the Teton landscape responds across the longest (10^{6-7} yrs) and shortest (10^{2-4} yrs) temporal scales. Long-term canyon incision rates determined from apatite (U-Th)/He (AHe) analysis of major drainages are highest (0.24 mm yr^{-1}) where measured uplift rates and duration are highest (near Mount Moran), leading us to propose that tectonic forcing operates as the first order control on long-term Teton erosion. Short-term denudation rates, which are derived by determining sediment volumes in Moran Bay that are deposited in catchments generated during the most recent glacial interval (Pinedale, ~15.5 ka), are 0.00303 – 0.4672 mm yr^{-1}. We compare these rates to previous work, which found that high rock fall rates (1.13-1.14 mm yr^{-1}) deposit large talus volumes in Avalanche and Moran Canyons. Despite their magnitude, such high rates of mass wasting are not sustained over long periods of time, as measured lake sediment volumes (0.007 km^3) are. We conclude that the Tetons are transport limited during the interglacial and large volumes of canyon sediment generated during this time cannot be moved absent the advance of valley glaciers. That is, fluvial systems in small mountain systems are substantially less effective than glaciers in denuding mountain topography.

KEYWORDS: Tectonics, Geomorphology, Landscape Response, Denudation Rates

Meredith Leigh Swallom

05/24/2019

DETERMINING RATES OF LANDSCAPE RESPONSE TO TECTONIC FORCING ACROSS A RANGE OF TEMPORAL SCALES AND EROSIONAL MECHANISMS: TETON RANGE, WY

By
Meredith Leigh Swallom

Dr. J. Ryan Thigpen
Director of Thesis

Dr. Ed Woolery
Director of Graduate Studies

05/24/2019

ACKNOWLEDGMENTS

The fact that this project is complete and I am in one piece is a testament to the efforts of many fantastic folks. A huge “thank you” must go first and foremost to my committee members, Drs. Thigpen, McGlue, and Woolery. When I had no idea what I wanted to pursue, y’all didn’t hesitate to let me take on this project and choose which pieces interested me and applied to my broader goals. Given that not one of you had seen me demonstrate any sort of competence or leadership in the field at that point, I still think you’re crazy for trusting me with a van full of people in the backcountry. Ryan, I won’t ever be able to thank you enough for your incredible mentorship over the last two years (but a Thigpen Endowment fund might be a start, eh?). No matter how behind schedule I was or how thoroughly Murphy’s Law applied on any particular day, you took everything in stride and encouraged me to do the same. I am a better scientist and calmer human being (believe it or not) thanks to you.

Many funding sources contributed to the success of this project as well. The departmental Ferm, Brown McFarlan, and Pirtle funds provided me with travel, analytical, and summer support, while the Overcash Gift Fund and the UWNPS seed grant were instrumental in ensuring a successful field season and an outstanding course experience for myself and many other students. Finally, the support of the Geological Society of America and the American Association of Petroleum Geologists was crucial for funding the thermochronologic analyses for this study.

I am forever grateful for the support and friendship of my fellow graduate students as well. Thanks to Bailee for always being there when I needed to vent or rage-walk to Starbucks, and to Brandon for being equal parts colleague, big brother, and

amusing angry grandpa-like figure. Your good attitude and sarcastic sense of humor never failed to make even the most stressful days A-ok. Rachel, thanks for never failing to be a shining beacon of pick-me-ups and compliments and for providing the refrigerator that housed the caffeine to which I owe at least 82% of my success. It was super cool of you to let me come crashing into your field area as the uncoordinated wonder I was. You da bomb. Many thanks also to Autumn for providing endless support, great stories, and hours of comic relief during our visit to the end of the earth.

To Summer, thanks for setting the stage for this work way back in the day at Tech, and for deciding to work in the prettiest place on the planet. We'd be nowhere (literally) without you. I also can't ever thank you enough for the various training and troubleshooting that never seemed to be necessary at a convenient time. Couldn't have gotten a single grain in the tubes without you.

Thank you to Pete for ensuring we always had a surplus of functional lab equipment and a fragrance-free workspace. Many samples would have gone undried and much sediment would have gone unvacuumed without you. And that accursed sink would still be clogged.

Finally, to Nathaniel. Thanks for sticking around Kentucky an extra couple years without complaint, for supporting me from afar while I was in Dallas for the summer, and for generally putting up with all the anxiety-ridden moments and not-so-pleasant days it took to get here. Looking forward to bluer skies, warmer days, and all the adventures ahead in Texas.

TABLE OF CONTENTS

ACKNOWLEDGMENTS iii
LIST OF TABLES vi
LIST OF FIGURES vii
CHAPTER 1. Introduction 1
1.1 Scientific Motivation 1
1.2 Teton Range Background and Study Approach 2
CHAPTER 2. Methodology 8
2.1 Study Design 8
2.2 Sample Collection Methods 9
2.3 Thermochronologic Analysis 11
2.4 Seismic Acquisition and Processing Methods 14
CHAPTER 3. Results 23
3.1 Thermochronology Results 23
3.2 Seismic interpretation and lake sediment volume calculations 30
3.3 Calculation of denudation rates from lake sediment 34
CHAPTER 4. Discussion 47
4.1 Identifying distinct stratal packages and possible key age boundaries 47
4.2 Determining short-term denudation rates from sediment volumes 49
4.3 Long-term incision rates from thermochronologic results 54
4.4 Comparison of short and long-term denudation rates 55
4.5 Implications of variability in multitemporal rates for denudation mechanics 56
CHAPTER 5. Conclusions and Future work 63
5.1 Key study findings 63
5.2 Knowledge gaps and future work 64
APPENDIX: Apatite Grain Photos and Measurements 68
REFERENCES 77
VITA 84

LIST OF TABLES

Table 3.1 Apatite He Dataset for Death Canyon....26
Table 3.2 Apatite He Dataset for Granite Canyon....27
Table 3.3 Apatite He Dataset for Paintbrush Canyon....28
Table 3.4 Apatite He Dataset for Avalanche Canyon....29
Table 3.5 Apatite He Dataset for Moran Canyon....29
Table 3.6 Volume Calculations of Key Sediment Packages....33
Table 3.7 Denudation Rate Calculations Using Lake Sediment....36
Table 4.1 Denudation Rate Calculations Using Canyon Sediment....53

LIST OF FIGURES

Figure 1.1 Project Approach 5
Figure 1.2 Geologic Setting of the Teton Range 6
Figure 1.3 Teton Range Previous Work 7
Figure 2.1 Bedrock Samples and Locations 16
Figure 2.2 Bedrock Sampling Locations in Outcrop 17
Figure 2.3 Mineral Separation Equipment and Procedures 18
Figure 2.4 Jackson Lake Average Annual Water Level 19
Figure 2.5 CHIRP Seismic Survey Grid 20
Figure 2.6 Sub-bottom Profiler and Cataraft Assembly 21
Figure 2.7 Moran Bay Line D19 Before and After Processing 22
Figure 3.1 TR-18-15 Mineral Separate 37
Figure 3.2 TR-16-01 Mineral Separate 38
Figure 3.3 TR-18-12 Bulk Sample and Separate 39
Figure 3.4 TR-18-11 Mineral Separate 40
Figure 3.5 Average AHe Ages of Analyzed Samples 41
Figure 3.6 Perched Moran Bay Sediment 42
Figure 3.7 Moran Bay Seismostratigrpahic Interpretation 43
Figure 3.8 Jackson Lake Total Sediment Isopach Map 44
Figure 3.9 Moran Bay Total and Recent Sediment Isopach Maps 45
Figure 3.10 Moran Bay Catchment Area Calculation 46
Figure 4.1 Modern Moran Bay Deltaic Accumulation 58
Figure 4.2 Line D19 Coring Targets 59
Figure 4.3 Stored Sediment Measurements 60
Figure 4.4 Synoptic Figure of AHe Ages for Incision Rate Estimates 61
Figure 4.5 Uplift Rate Trends Along Strike 62
Figure 5.1 Future Bedrock Samples 66
Figure 5.2 Jackson Lake Coring Targets 67

CHAPTER 1. INTRODUCTION

1.1 Scientific Motivation

Understanding how landscapes respond to changes in tectonic and climatic forcing remains as one of the most enigmatic challenges in tectonics, landscape dynamics, and geomorphology (Whittaker, 2012; Godard et al., 2013). Specifically, the rates at which landscape erosion and exhumation responds to transient changes in forcing (such as fault slip and subsequent tectonic uplift) remains poorly constrained. Numerous studies have attempted to quantify the relative contributions of climate and tectonics on landscape evolution using a variety of approaches. For example, Godard et al. (2013) used a Himalayan transect to demonstrate that cosmogenically derived denudation rates vary absent of variation in precipitation rates, suggesting that rock uplift rate is the dominant control of denudation rates in that system. This interpretation is, to some degree, corroborated by a number of numerical modeling studies that highlight the inability of climate to exert a first-order control on the evolution of a tectonic system (Godard et al., 2006; Roe and Brandon, 2011). Alternately, multiple studies use numerical modeling to demonstrate that atmospheric processes can fundamentally influence the tectonic evolution of active systems (Willett, 1999; Konstantinovskaia and Malavieille, 2005; Whipple and Meade, 2006; Whipple, 2009), although each of these studies concede that definitive field evidence of climate-modulated tectonics is lacking (Whipple, 2009). Because this enigma persists primarily due to a lack of integration across timescales and mechanisms, it is necessary to identify an ideal natural laboratory where the signals that define uplift, incision, and sediment flux rates can be separated at multiple time and length scales (e.g., Dadson et al., 2003; Figure 1.1).

1.2 Teton Range Background and Study Approach

The Teton Range, which is located in northwestern Wyoming, lies at the confluence of four distinct tectonic provinces: the Sevier fold and thrust belt, the Laramide uplift, the Snake River plain, and the Basin and Range province (Figure 1.2). Despite its complex setting, the Teton Range is a relatively simple tectonic system. The range, which represents the uplifted footwall block of the Teton normal fault, is ~70 km in length (Tranel et al., 2011). Because of this, it serves as an ideal natural laboratory for filtering the complex interplay between uplift and climate-controlled erosional mechanisms, as climate can be reasonably assumed to vary little along strike and is mostly considered to be a function of elevation in this system.

Further, recent bedrock thermochronologic studies have produced a refined understanding of the variability in fault slip rates along strike (Brown et al., 2017, Hoar et al., 2019). Those studies used apatite (U-Th)/He thermochronology (AHe) of samples collected along subvertical footwall transects from the eastern range front to demonstrate that Teton fault slip originated in the northern part of the range at Mount Moran at 15-13 Ma, with fault motion onset becoming younger to both the north and south at Eagles Rest Peak (~9 Ma) and Grand Teton (~10 Ma), respectively (Figure 1.3). This documented variation in tectonic forcing along-strike in the Teton Range provides a unique opportunity for examining how variations in tectonic forcing may influence landscape response through time. Additionally, the Teton Range clearly preserves the effects of both glacial and fluvial erosion mechanisms, thus allowing the magnitude and efficiency of each of these mechanisms to be separated and analyzed.

Although previous studies within active systems present convincing evidence of the relative contributions of tectonics and climate to overall landscape evolution, more work remains to be done in order to definitively determine the degree to which climate and tectonic forcing control landscape response across a range and spatial and temporal scales. To address some of these challenges, we have designed a study that allows us to: (1) compare long- and short-term temporal windows of incision, and (2) compare the efficiency of glacial versus fluvial mechanisms of erosion in active tectonic systems. To do this, we first compare lag times between fault slip onset and incision of several major Teton Range drainages to determine how long-term (10^7 yrs) incision varies with variability in rock uplift rate and duration along strike (e.g., Brown et al. 2017). We then compare these long-term response estimates with intermediate-term (10^4 yrs) landscape response determined by measuring postglacial sediment efflux in Moran Bay, Jackson Lake.

Next, we determine a potential short-term (10^2 yrs) landscape response rate by measuring the volume of a Moran Bay sediment package identified in seismic reflection data that potentially resulted from an increased lake level following emplacement of Jackson Dam in 1911. If response rates scale appropriately along strike and through time with such tectonic forcing, it will be clear that within the Teton Range, tectonic forcing operates as the first-order control on the landscape response. If rates do not scale, then it is likely that climate, and more specifically climatically controlled mechanisms such as glaciation, are more influential controls on Teton landscape evolution than previously thought. Lastly, we highlight knowledge gaps that persist and present recommendations

for future bedrock sampling and coring locations that will allow for development of more robust age constraints.

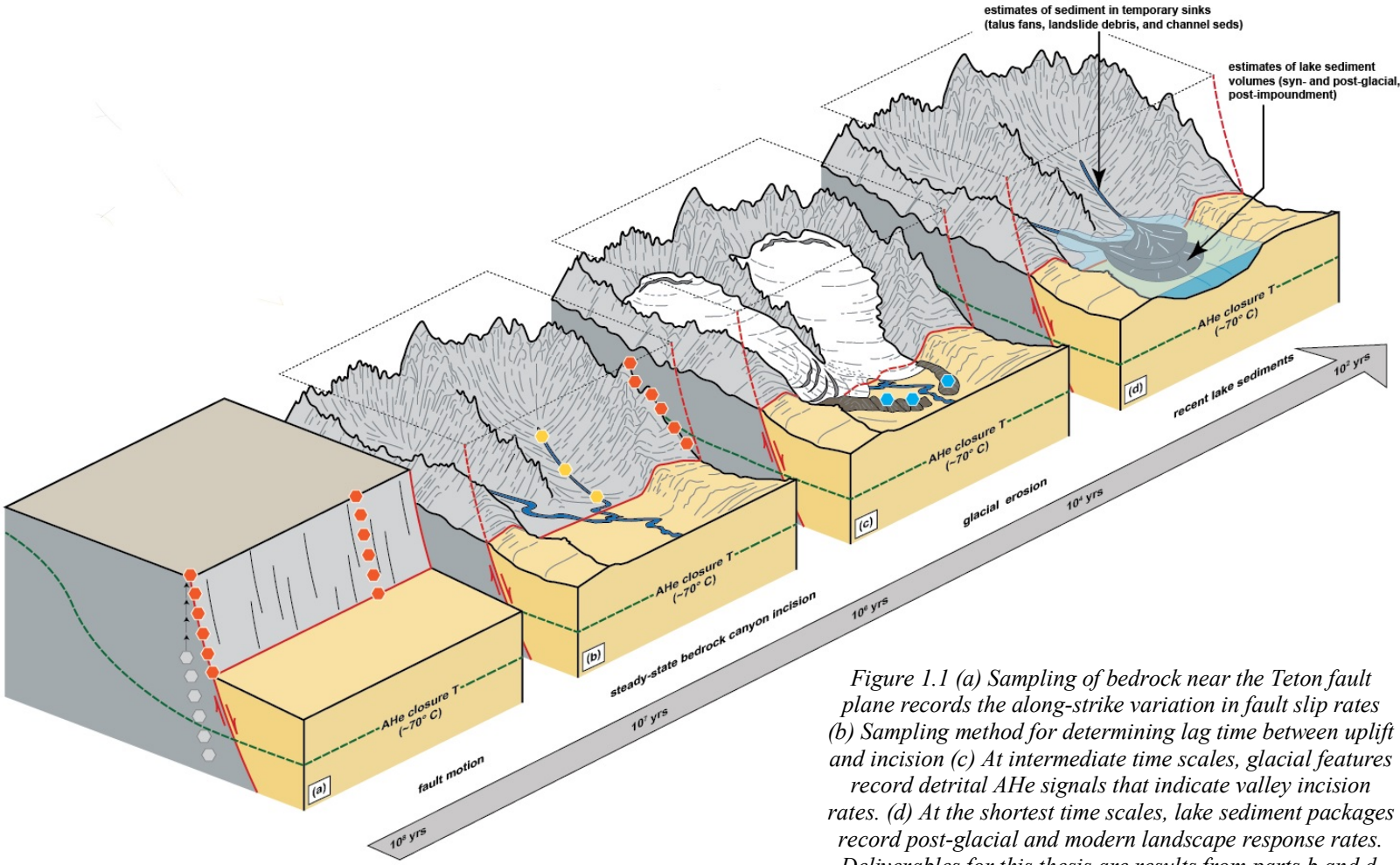

Figure 1.1 (a) Sampling of bedrock near the Teton fault plane records the along-strike variation in fault slip rates (b) Sampling method for determining lag time between uplift and incision (c) At intermediate time scales, glacial features record detrital AHe signals that indicate valley incision rates. (d) At the shortest time scales, lake sediment packages record post-glacial and modern landscape response rates. Deliverables for this thesis are results from parts b and d.

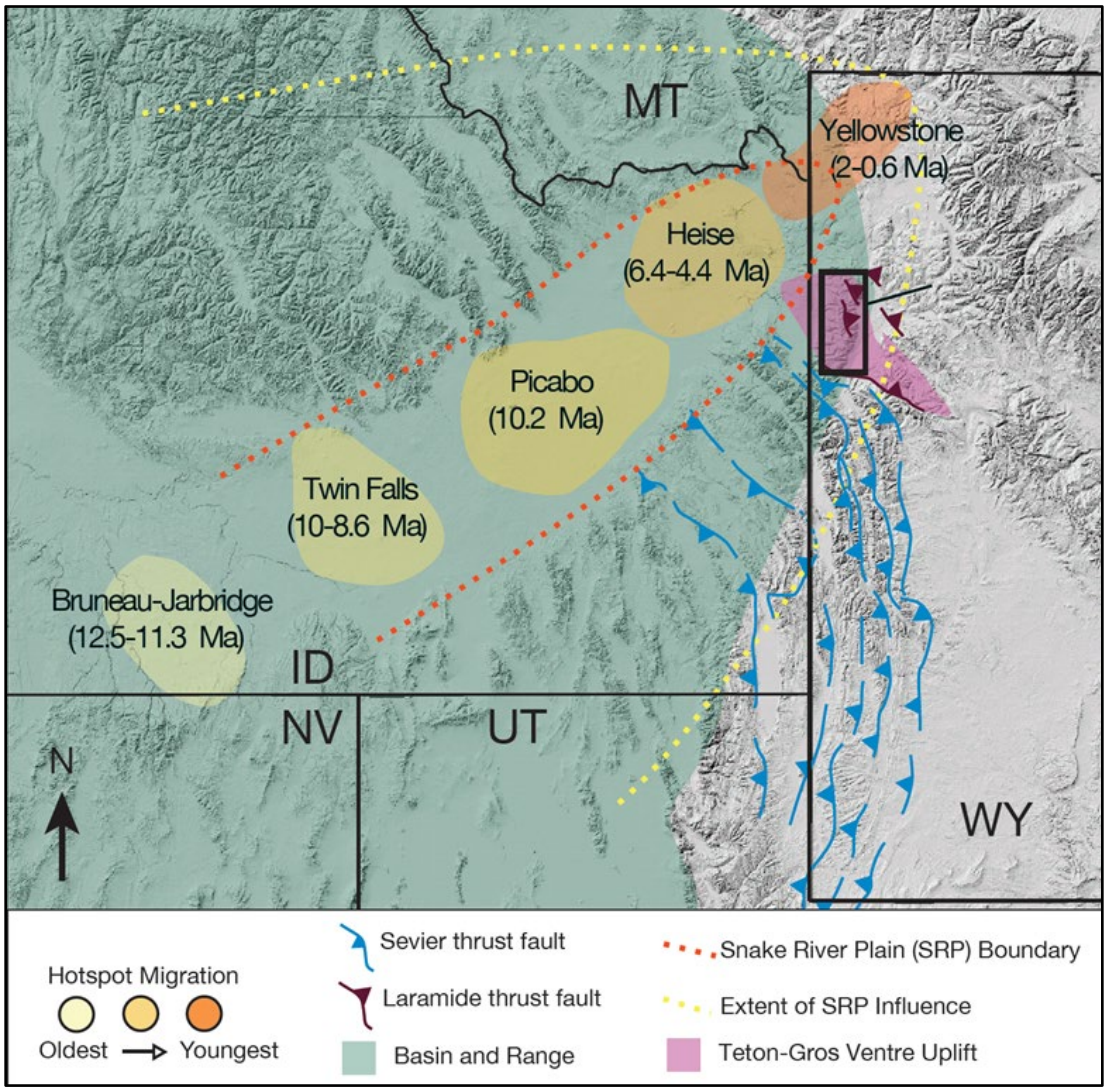

Figure 1.2 - Digital elevation model (DEM) of the greater Teton-Yellowstone region that highlights the confluence of multiple geologic provinces, including the Teton Range (black box), the Laramide fold-thrust belt, and the Snake River plain, which represents the track of the Yellowstone hotspot.

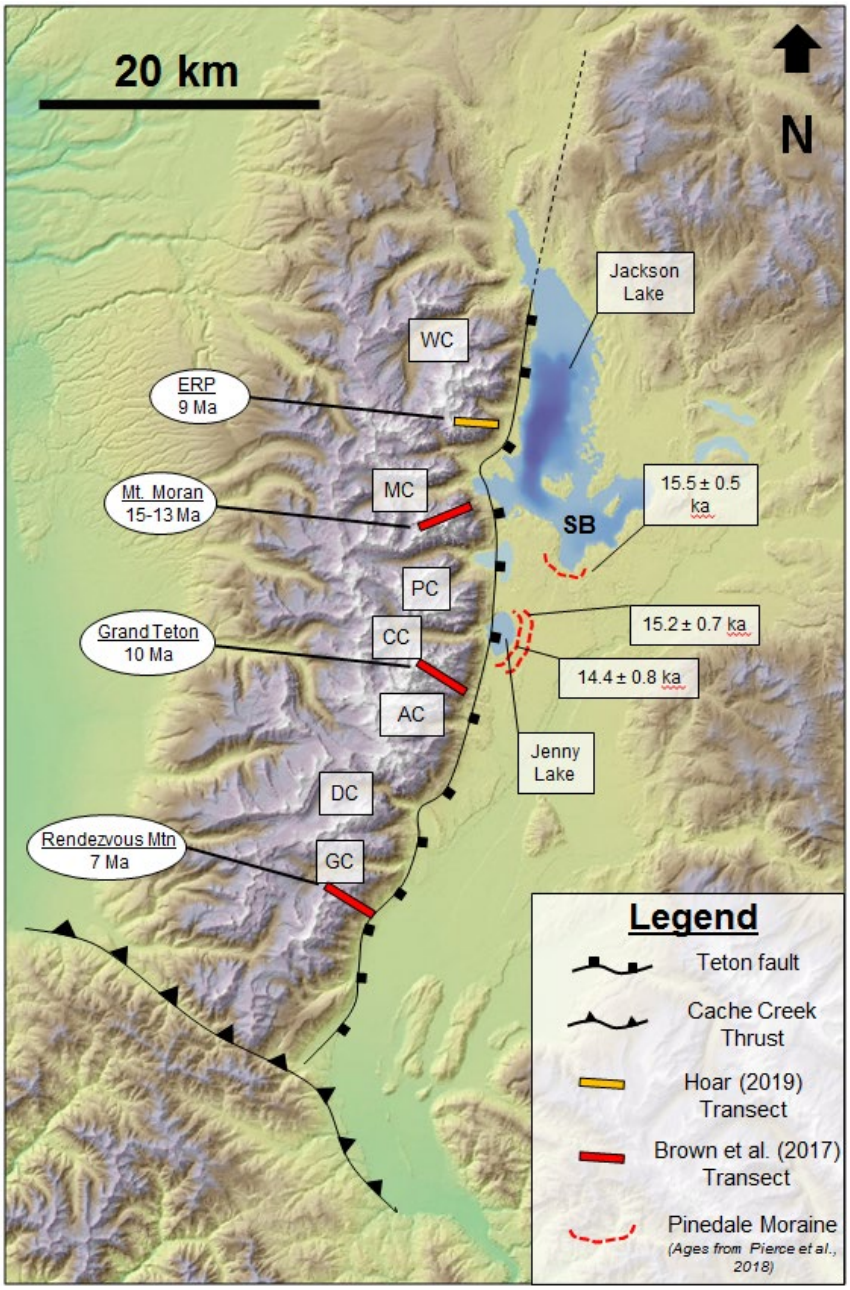

Figure 1.3 – Teton Range previous work. Transects (ERP, Moran, Grant Teton, Rendezvous) reveal slip onset timing and ^{10}Be ages of Pinedale moraines yield ages of scour of Jackson and Jenny Lake and onset of postglacial sedimentation.. Major canyons serve as conduits for sediment flux into lakes. SB: Spalding Bay.

CHAPTER 2. METHODOLOGY

2.1 Study Design

Over the longest temporal scales, landscape response in the Teton Range is recorded primarily by incision of major glacial and fluvial transaxial drainages, which serve as significant conduits for erosional sediment flux (Milliman and Syvitski, 1992) into glacial range front lakes (Figure 1.3). Due to its relatively low closure temperature (60-70° C), apatite (U-Th)/He thermochronology (AHe) is useful for constraining timing of incision occurring in the upper 2-3 km of the crust (Stockli, 2005; Spotila, 2005; Ehlers, 2005). Obtaining AHe ages of the bedrock in the lowest portions of these canyons is a key component of this study, as the lag time between onset ages of fault motion (Brown et al., 2017) and the AHe cooling ages in the low elevation parts of these drainages can yield estimates of the total amount of time necessary to incise the canyons, which should represent the longest term (10^7 years) landscape response (Figure 1.1b). The rugged peaks and valleys of the Teton Range are predominantly composed of highly resistant Archean basement and are thus well suited for AHe age analysis. The theory that underpins this idea is discussed in detail with examples in the following section.

In the Teton Range, the intermediate scale of landscape response is recorded by the erosional efflux into glacial lakes that formed at ~15 ka (Pierce et al., 2018) along the eastern range front. By using high-resolution seismic reflection data collected on these lakes, it is possible to measure sediment volumes and thus provide a means of estimating efflux over known time periods (Figure 1.1d), as the ages of each major range front lake have been well constrained through cosmogenic dating of both lateral and terminal moraines that impound these lakes (Pierce et al., 2018). Ancient sedimentation in Jackson

Lake is constrained by the Pd-2 and Pd-3 phases of Pinedale glaciation (15.5 – 14.4 ka) which scoured the present-day basin. Terminal moraines south of Spalding Bay (Figure 1.3) have ^{10}Be ages of ~15.5 ka (Pierce et al., 2018), which serves as a likely onset age for postglacial sedimentation in Moran Bay, which is one of the key focus areas for this study.

Using the lake seismic reflection data, we aimed to determine landscape response on the shortest temporal scales. Because Jackson Dam was erected in 1911, producing a significant lake level rise (~7.5 m), Jackson Lake is well-suited for studying the variability in sedimentation rates over timescales ranging from 10^2 to 10^4 yrs where both a postglacial transitional surface (15.5 ka) and pre-dam impoundment surface (~100 years) are preserved.

2.2 Sample Collection Methods

The first objective of this work was to determine the long-term (10^7 years) landscape response (Figure 1.1b) of the Teton Range recorded by incision of the major transaxial canyons. Theoretically, this response time should be recorded as the 'lag' between onset of fault motion along a particular segment of the fault and the incision-related cooling recorded in an adjacent transaxial canyon, assuming that incision is of substantial magnitude to exhume material that was at a temperature greater than the AHe systems that are reset (i.e., samples with AHe ages younger than the age of fault slip onset). For example, a subvertical AHe transect from Brown et al. (2017) demonstrated that fault slip onset occurred at 15-13 Ma at Mount Moran (Figure 1.3). So, this idea predicts that if incision in the adjacent canyons (in this case Moran Canyon) is the result of uplift due to faulting, that incision should record a younger cooling age than the onset of fault slip, as the incision occurs after fault-related uplift. This difference between the

younger incision cooling age and the older fault slip onset age is the 'lag' and presumably represents the long-term incision rate and thus the entire finite incision history averaged over multiple glacial and interglacial cycles. Alternately, when low elevation canyon samples do not yield AHe ages that are younger than fault slip onset ages derived from modeling, total exhumation magnitude can be estimated by comparing the sample elevation to that of the paleo-partial retention zone (PRZ; 60˚-70˚C), which, for the purposes of this study, was assumed to have been at a depth of ~1.8 km, considering a typical geothermal gradient of 25˚C km^{-1} and a surface temperature of 25˚C.

Because we expected the youngest AHe ages to be preserved at the lowest elevations, bedrock samples were collected at the lowest possible elevations in major range-front incised drainages (Figure 2.1) Also, samples were collected at least 1-2 km from the canyon mouths, which are interpreted to lie close to the projected fault scarp, in an effort to avoid complex thermal field effects that may occur due to fault-related warping of isotherms. Proximity to previously analyzed range-front subvertical transects of Brown et al. (2017; Rendezvous, Grand Teton, Mount Moran) and Hoar (2019; Eagles Rest Peak) was also considered to ensure the opportunity to determine 'lag' time between uplift and incision.

One sample was collected in Moran Canyon in 2008 as part of a previous thermochronologic study (Brown et al., 2017). In 2016, two samples were obtained in Cascade Canyon and one sample was collected in Webb Canyon in the northernmost part of the range. In 2017, two samples were collected in Death Canyon in the southern part of the range, and ten other canyon samples were collected in August of 2018 in Death (*n=2*), Paintbrush (*n=4*), Avalanche (*n=1*), and Granite (*n=3*) Canyons (Figure 2.1). Selection of

all samples was made on the basis of most suitable lithologies for apatite yield (granites, banded gneisses, and quartz monzonites) and confidence that the outcrop being sampled was *in situ*. Periglacial processes and mass wasting events in the range are capable of displacing massive blocks from higher elevations and mistaking these large boulders for *in situ* exposures has the potential to result in erroneously old AHe ages, as older AHe samples are displaced to lower elevations in a normal fault system such as this one. Additionally, obviously weathered or hydrothermally altered outcrops were avoided wherever possible.

2.3 Thermochronologic Analysis

Several stages of processing were necessary to isolate apatite grains for AHe analysis (Figure 2.3). First, bedrock samples were crushed with a hammer into pieces ~4 cm in diameter prior to jaw crushing in the rock processing facility at the Kentucky Geological Survey. After crushing, the samples were further disaggregated to sand size particles using a diskmill (2016 and 2017 samples) or a rotary hammermill (2018 samples). Use of the hammermill replaced the diskmill in 2018 after Hoar (2019) determined that the shearing force of applied by the diskmill abraded Teton apatites so that they were difficult to identify and concealed potential inclusions by increasing surface roughness.

During milling, samples were sieved through a 250 micron sieve cloth, and the coarse separate was milled again to reduce the entire sample to a grain size <250 microns. Following milling, the sample was density separated using a Wilfley-style water shaker table to remove small (<50 micron) dust particles and lower density mica grains. The

dense separate was then dried using acetone and a vacuum flask to prevent oxidation, and the low density separate was discarded.

Following Wilfley table separation, heavy liquids separation was performed on each sample to separate denser grains (including apatite at 3.2 g/cm^3) from the less dense majority of the rock volume, which was predominantly quartz and feldspar (~2.7 g/cm^3). Acetylene tetrabromide (ATB) was used as the primary heavy liquid in this study due to its intermediate density of ~2.95 g/cm^3. The heavy ATB 'sink' separate was then magnetically separated using a Frantz instrument at progressively increasing amperage intervals of 0.1, 0.5, 1.0, and 1.8.

The final sample yield (1.8 amp Frantz separate) was examined under a Leica M165 C microscope to distinguish between apatite and zircon grains, as both exhibit high relief and are similar in morphology when the grains are slightly rounded or abraded. Care was taken to select only grains without major birefringent zoning or inclusions, as inclusions cannot be identified accurately in most cases and can have effects on the measured helium in the whole grain if they contain U, Th, or He (e.g., zircon inclusions). Additionally, morphological characteristics and grain size measurements were recorded for each grain picked, as the grain shape and dimensions influence the correction parameters applied after a raw AHe age is determined (Farley et al. 1996). Several grains for each sample were packed as single grains in niobium (Nb) tubes as opposed to multi-grain aliquots so that any erroneous ages could be culled after analysis.

All samples were analyzed at the University of Illinois Urbana-Champaign Helium Analysis Laboratory (HAL) under the direction of Dr. William Guenthner. First, each grain was outgassed for ^{4}He using an in-vacuum extraction line that is heated with a

Nd:YAG laser. Nb packets were heated at approximately 1000°C for three minutes to extract ^{4}He. Following extraction, the crystal was spiked with ^{3}He and analyzed on a quadrupole mass spectrometer. Line gas standards as well as Durango fluorapatite gas standards were analyzed after every 4-6 aliquots to monitor instrument performance. Following ^{4}He outgassing and mass spectrometry, grains were unpacked from the niobium tubes and dissolved in HNO_3 at 90°C. After one hour of dissolution, grains were equilibrated and spiked with ^{223}U-^{229}Th-^{147}Nd-^{42}Ca. U, Th, and Sm concentrations were measured using a Thermo iCAP Q ICP-MS. These concentrations and the measured ^{4}He from the first stage of analysis were applied to

$$Eq.\ [1]\quad {}^{4}He = 8^{238}U[e^{\lambda 238t} - 1] + 7^{235}U[e^{\lambda 235t} - 1] + 6^{232}Th[e^{\lambda 232t} - 1] + {}^{147}Sm[e^{\lambda 147t} - 1]$$

to determine t, or the raw AHe age for each grain. Axial and radial grain measurements were then used to apply an alpha ejection correction to the raw AHe ages and determine a final AHe age for each sample grain. Because individual apatite grains yield their own AHe age through these methods, multiple grains were packed and analyzed for each bedrock sample. Typical thermochronologic studies recommend analyzing a minimum of 2-10 grains to ensure a meaningful age (Peyton and Carrapa, 2013). Because Teton apatite grains tend to vary greatly in their quality within a single sample, we analyzed a minimum of 8-10 grains where possible for each bedrock sample in order to reduce uncertainty in the average AHe ages.

2.4 Seismic Acquisition and Processing Methods

The second objective of this study was to determine the intermediate and short-term (10^4 - 10^2 yrs) landscape response (Figure 1.1d) recorded in lake sediment packages along the range front to compare with long-term rates derived from AHe canyon incision analyses. Previous work (Smith et al., 1993; Larsen et al., 2016) has shown that both glacial and postglacial sediment packages are preserved in Teton range-front lakes following glacial scouring of these basins in Pd-2 (15.5 ± 0.5 ka) and Pd-3 (14.4 ± 0.8 ka) time (Pierce et al., 2018). Further, the construction of Jackson Dam in 1911 resulted in a lake level rise of ~7.5 meters and generation of accommodation space for increased sedimentation (Figure 2.4). Where the notional pre-dam impoundment surface ("Dambrian") is preserved and imaged in seismic section it is possible to measure sediment volumes above it to determine modern (i.e., <100 yr) response rates. Similarly, where a transitional surface marking the end of the glacial interval is imaged, volumes of sediment on the 10^4 yrs timescale can be determined. Thus, in Jackson Lake, distinct sediment packages are preserved that record a range of temporal 'windows' of erosional flux through the postglacial and modern timescales.

In order to identify these key sediment packages and estimate sediment volumes within Jackson Lake, a grid of 54 high-resolution CHIRP seismic profiles (Figure 2.5) was collected in August of 2018 using a cataraft assembly and an Edgetech SB-0512i CHIRP sub-bottom profiler with a model 3200 topside processor and integrated dGPS (Figure 2.6). The cataraft velocity during acquisition was ~3 kts, with shot points collected every 2 seconds. Data was collected at a swept frequency range of 0.4-4.0 kHz to optimize both penetration of the sediment packages and image resolution. Digital

signals were recorded as SEGY files, which were then imported into Seisware for processing and interpretation. Each seismic profile was processed using a bandpass filter with variable frequency cut offs and an amplitude gain with a bulk gain of one and gain exponent of 2 was applied to improve image quality (Figure 2.7). Following processing, a depositional chronology for one key Moran Bay line (D19) was established by mapping distinct sediment packages bound by reflector truncations.

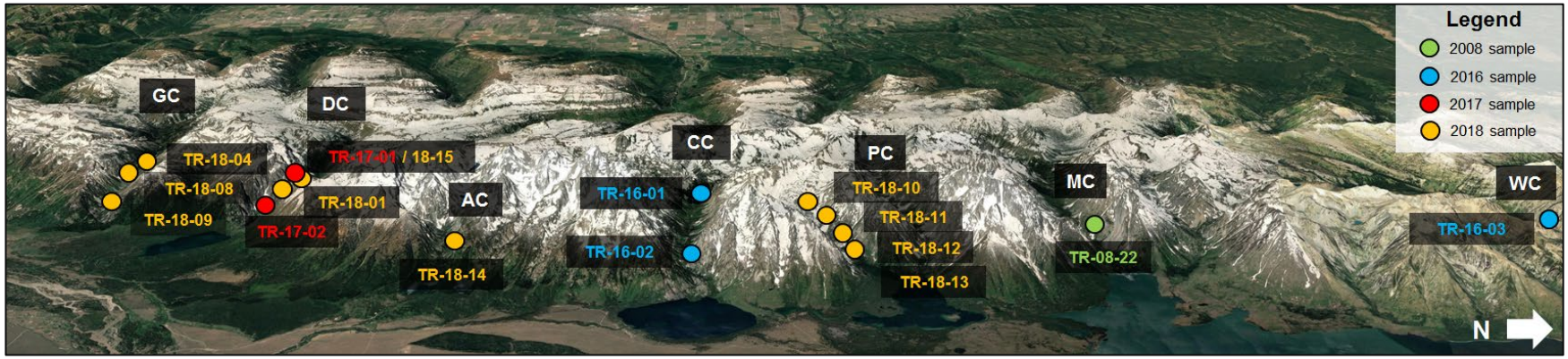

Figure 2.1- Bedrock sampling locations for AHe age analysis of major Teton incised drainages: Granite Canyon (GC), Death Canyon (DC), Avalanche Canyon (AC), Paintbrush Canyon (PC), Moran Canyon (MC), and Webb Canyon (WC). Green, blue, red, and orange samples collected in 2008, 2016, 2017, and 2018 field seasons, respectively.

Figure 2.2 – Bedrock sampling locations in outcrop. a) TR-18-01 in Death Canyon with trekking pole for scale. b) TR-18-12 in Paintbrush Canyon with hammer for scale. c) TR-18-09 collected in Granite Canyon from large roche moutonnée feature.

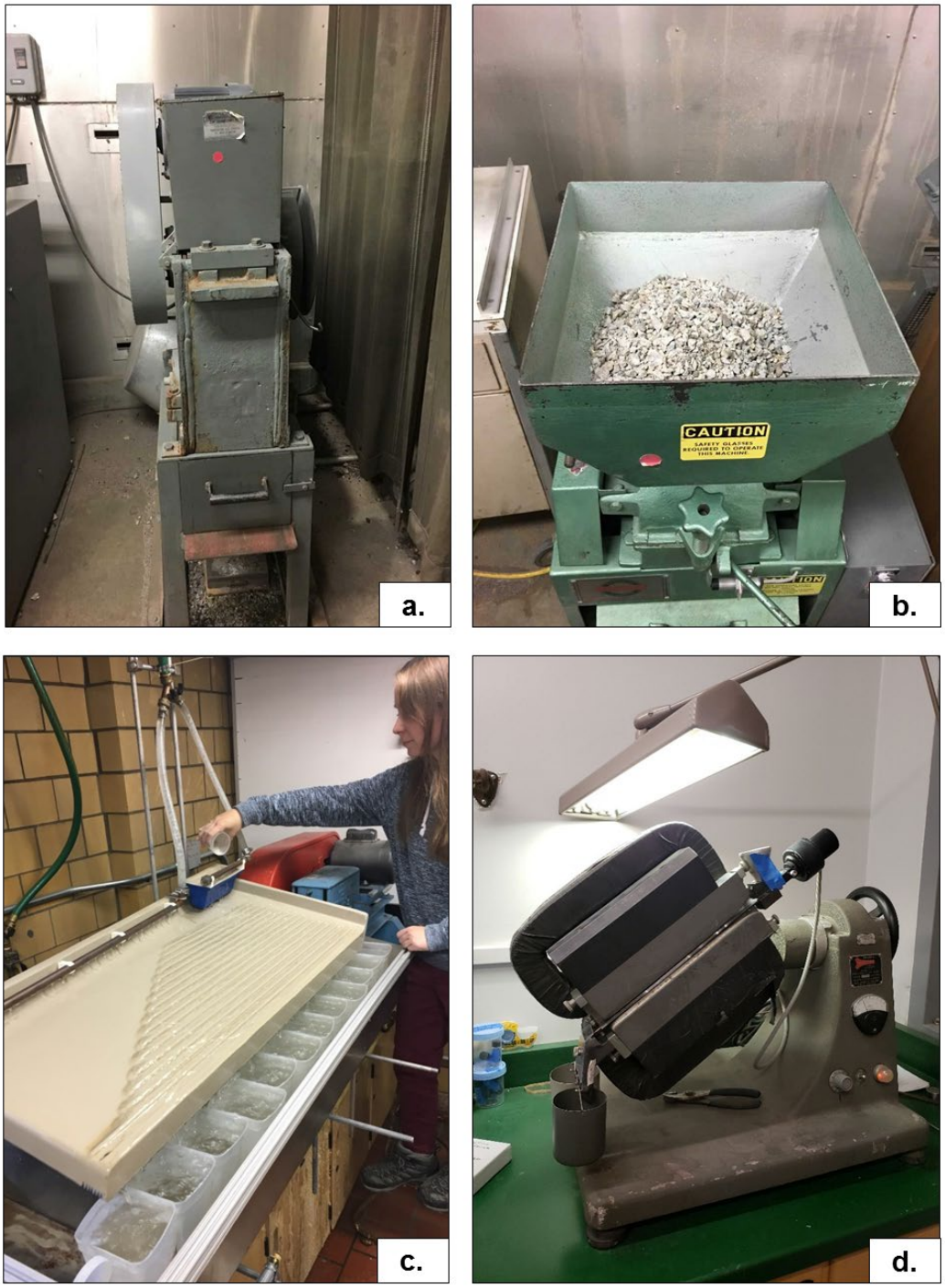

Figure 2.3 – Mineral separation equipment. a) jawcrusher and b) hammermill at Kentucky Geological Survey. c) Wilfley table for small dust and mica removal. d) Frantz instrument.

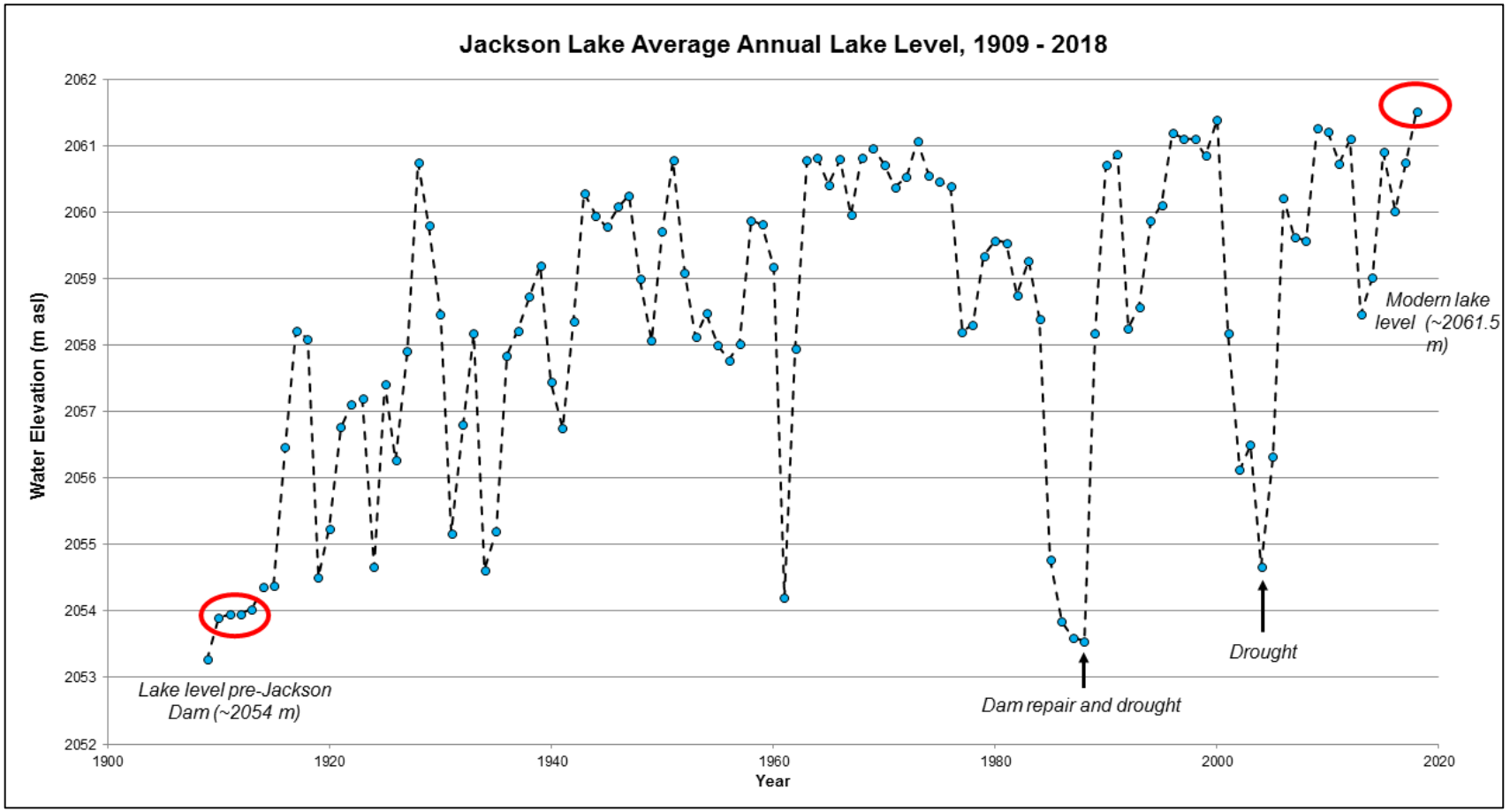

Figure 2.4 – Average annual water level at Jackson Lake from 1909 to 2018. Fluctuations reflect periodic dry seasons, with net lake level increase of ~7.5 m since the emplacement of Jackson Dam.

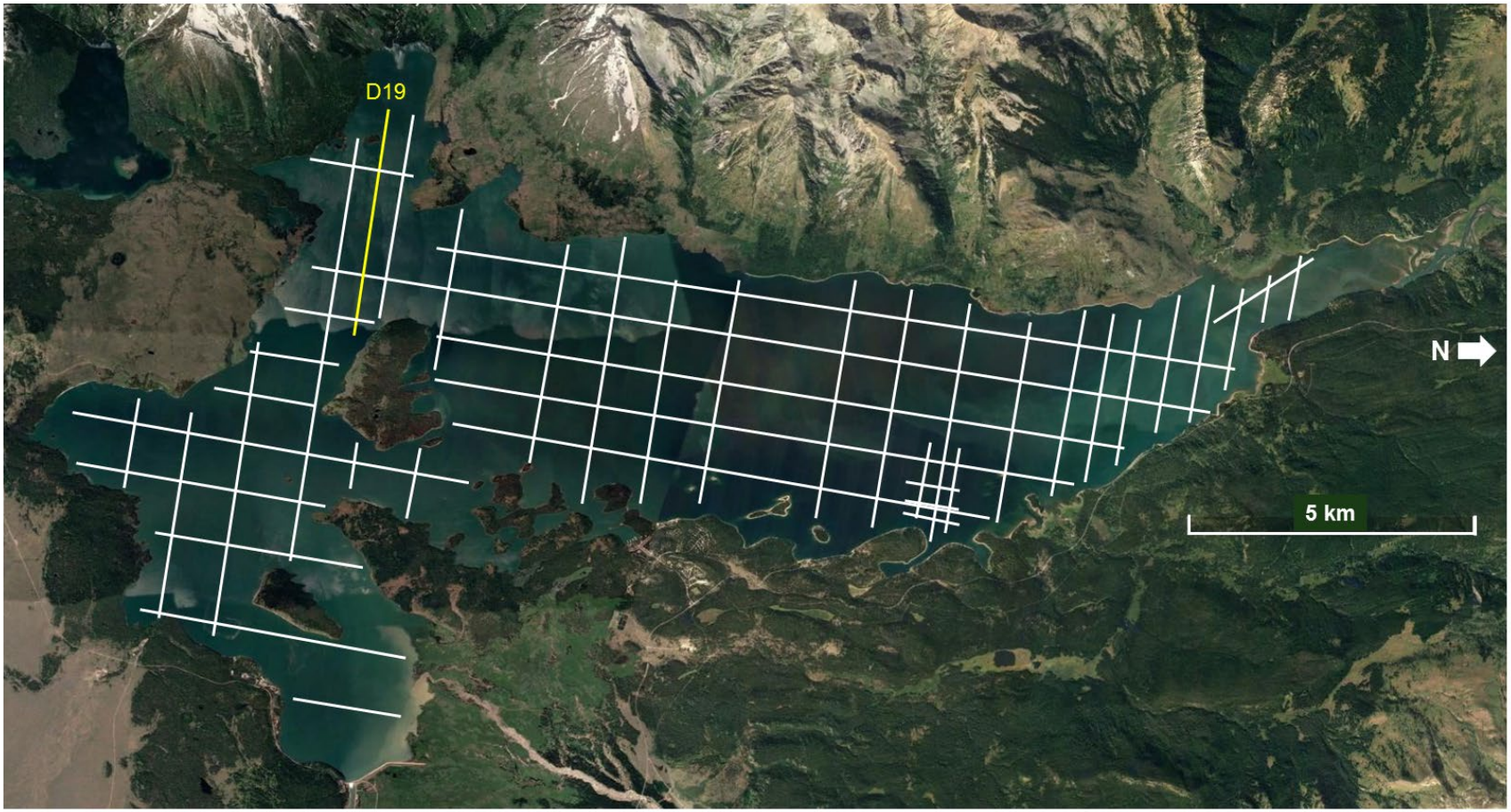

Figure 2.5 - CHIRP survey grid of Jackson Lake, acquired August 2018. Moran Bay line D19 shown in yellow.

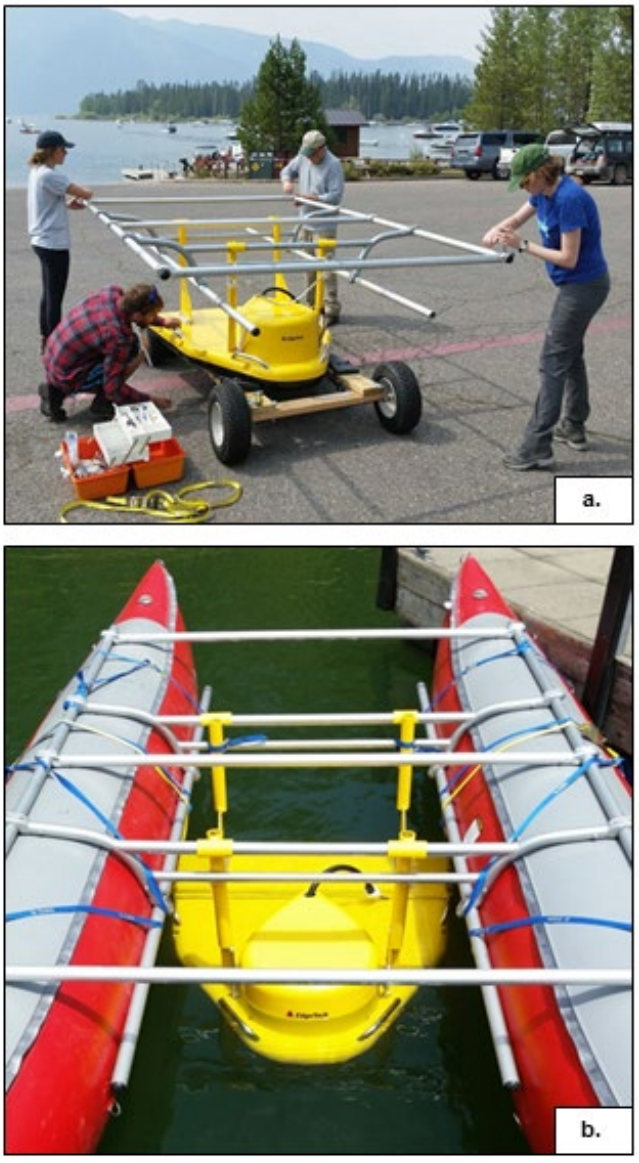

Figure 2.6 – a) Edgetech sub-bottom profiler attached to cataraft assembly and b) sub-bottom profiler with inflatable pontoons

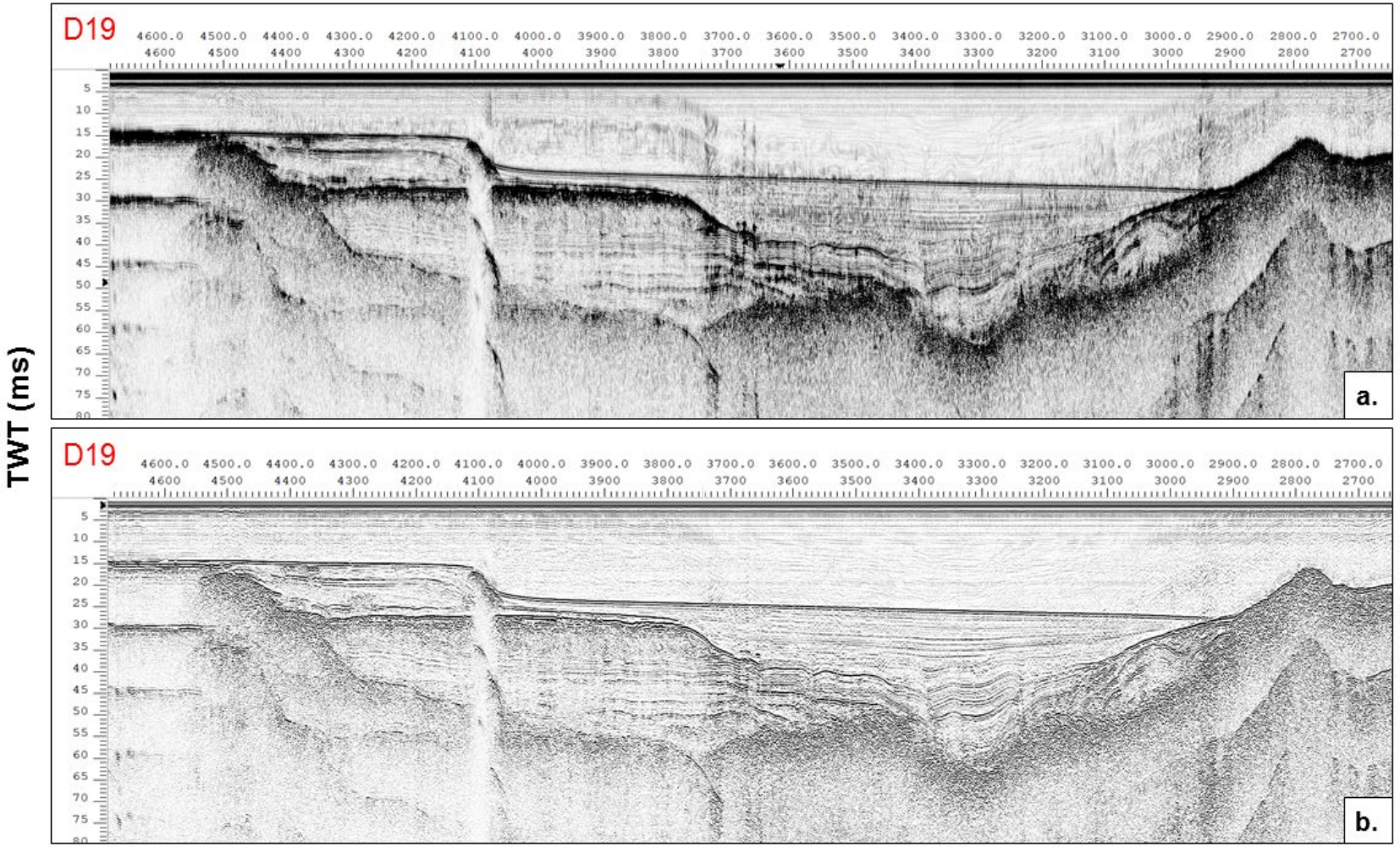

Figure 2.7– Moran Bay line D19. a) Before application of bandpass filter and amplitude gain and b) after processing workflow. Line location shown on survey grid in Figure 2.5.

CHAPTER 3. RESULTS

3.1 Thermochronology Results

When examining mineral separates, we found the most whole apatites in the Death Canyon samples (TR-17-01/TR-18-15, TR-18-01), which were layered gneisses (Figure 3.1) and quartz monzonites. Similarly, whole apatites were found in the separate for Granite Canyon samples from the Rendezvous Metagabbro, though grains tended to be comparatively more abraded.

There were notable differences in yield quality amongst samples collected in different years, which we attribute to the previously discussed adjustment in processing procedures. Samples from 2016 and 2017 were diskmilled while the 2018 samples were hammermilled. The diskmilled samples (TR-16-01, TR-16-02, TR-16-03) tended to contain far fewer, if any, whole apatite grains in the final separate (Figure 3.2). Despite being processed on the hammermill instead of the destructive diskmill, granitic Paintbrush Canyon samples tended to have the poorest and most fractured yields of all (Figure 3.4) with the exception of the more gneissic TR-18-12 (Figure 3.3). We therefore suggest that lithology exerts primary control on the morphology of grains in the final separate regardless of processing methodology, so banded gneisses and quartz monzonites should be sampled wherever possible as opposed to felsic intrusive suites.

Though our initial AHe sampling suite was comprised of 16 bedrock samples (Figure 2.1), only eight samples were selected for AHe analysis due to the yield quality issues discussed above. We therefore revised our methodology to focus on analyzing more grains from fewer samples, with the intent of reducing uncertainty in our analyses. One sample (TR-17-02) was later determined to have been collected an insufficient

distance (~0.87 km) from the present day fault scarp to yield a reliable age, and eight samples did not yield apatites of sufficient quality for analysis. Samples with grains selected for analysis and their AHe age results are shown by location in Figure 3.5. Because two of these were sampled from the same locality in 2017 and 2018 (TR-17-01, TR-18-15), we selected grains from each and average them as one sample.

After both stages of analysis at the University of Illinois Urbana-Champaign, raw AHe ages calculated using Equation 1 were corrected for helium particle alpha ejection using the radial and axial grain measurements. Corrected AHe ages from all individual apatites from Granite, Death, Avalanche, Paintbrush, and Moran Canyons range from 91.35 Ma to 3.66 Ma. We calculated an average AHe age for each sample from these individual corrected grain ages and report these and standard deviations for each sample in Tables 3.1 – 3.5.

In Death Canyon (Table 3.1), average AHe ages for two bedrock samples (TR-17-01/TR-18-15 and TR-18-01) are 42.2 ± 27.5 Ma (9 grains analyzed) and 12.8 ± 4.0 Ma (using 8 suitable grains). In Granite Canyon (Table 3.2), AHe ages averaged from multiple aliquots at two sampling localities (TR-18-04 and TR-18-09) ranged from 32.6 ± 4.4 Ma to 23.9 ± 23.5 Ma from 9 and 7 grains, respectively.

Sample TR-18-12 collected in Paintbrush Canyon (Table 3.3) had 10 grains selected for analysis, with an average age of 7.7 ± 2.1 Ma. Similarly, Avalanche (Table 3.4) and Moran Canyon (Table 3.5) samples (TR-18-14 and TR-08-22, respectively) have average AHe ages of 25.2 ± 5.0 Ma (6 grains) and 8.0 ± 0.6 Ma (4 grains).

Though Tables 3.1–3.5 report an AHe age for each grain sent for analysis at the University of Illinois Helium Analysis Laboratory, samples marked with an asterisk (*)

were culled after analysis due to visible grain quality issues (e.g. significant fractures or irregular shape) or severely anomalous age results compared to other grains of the same sample. These anomalous grains were not included in the calculated average ages reported here but are included to provide transparency for our culling process.

Table 3.1. Apatite-He dataset for Death Canyon

Death Canyon											
Sample	Elev (m)	Length (µm)	Width (µm)	He atoms	U (ppm)	Th (ppm)	Sm (ppm)	Raw Age	Corrected Age	Avg Age	Std Dev
TR-18-01-01	2267	202.0	127.0	1894193000	5.0	3.3	97.9	9.47	11.80	**12.8**	4.0
TR-18-01-02		268.0	161.0	188363271600	92.6	76.5	43.2	23.52	27.89*		
TR-18-01-03		169.0	127.0	14001195600	29.8	16.0	303.8	14.54	18.33		
TR-18-01-04		187.0	155.0	28613120200	8.4	4.6	152.3	63.05	76.32*		
TR-18-01-05		201.0	148.0	7623427000	14.3	12.8	168.8	9.49	11.56		
TR-18-01-06		181.0	128.0	5719963200	14.0	6.5	225.5	11.73	14.68		
TR-18-01-07		182.0	151.0	13050818200	14.1	7.8	148.4	18.74	22.83*		
TR-18-01-08		149.0	123.0	3767135400	23.4	14.1	255.7	5.94	7.61		
TR-17-01-1	2435	301	205.55	53095798000	10.901	4.088	286.09	32.79	37.41	**42.2**	27.5
TR-17-01-2		324	225.595	88404302000	12.763	4.1497	173.73	36.78	41.49		
TR-18-15-1		334	166.017	103814298000	22.832	11.438	304.22	41.84	48.85		
TR-18-15-2		251	168.57	76539484000	15.609	7.173	205.49	58.58	69.00*		
TR-18-15-3		281	193.01	81525248000	14.143	4.0234	175.75	48.93	56.37*		
TR-18-15-4		350	182.356	360673250000	32.717	17.867	363.5	79.26	91.35		
TR-18-15-5		159	172.552	9132942000	14.284	10.975	215.21	10.80	13.04		
TR-18-15-6		222	171.75	9583840000	6.6858	4.3035	164.72	17.77	21.01		
TR-18-15-7		226	155.788	10536806000	11.987	4.2606	195.53	13.94	16.67*		

Table 3.2. Apatite-He dataset for Granite Canyon

Granite Canyon											
Sample	Elev (m)	Length (µm)	Width (µm)	He atoms	U (ppm)	Th (ppm)	Sm (ppm)	Raw Age	Corrected Age	Avg Age	Std Dev
TR-18-04-1	2383	253	196.77	19011762000	4.0385	3.925	3.493	37.46	43.43*	**32.6**	4.4
TR-18-04-2		297	144.758	31939712000	18.082	7.0588	17.411	24.90	29.80		
TR-18-04-3		229	186.154	47161342200	18.982	13.752	14.191	25.61	30.00		
TR-18-04-4		176	168.58	31870482000	14.593	19.885	11.219	31.66	38.24		
TR-18-04-5		150	179.977	340799424000	194.47	285.16	58.817	25.76	31.22		
TR-18-04-6		134	128.265	2302048000	9.6148	4.1631	20.933	9.45	12.11*		
TR-18-04-7		203	129.467	171365922000	123.67	139.91	71.986	30.75	38.36		
TR-18-04-8		163	151.753	98229544000	72.317	81.909	53.143	27.38	33.73		
TR-18-04-9		218	146.592	7319116000	5.9787	3.3346	18.246	22.11	26.80		
TR-18-09-1	2234	286	187.37	5468568000	8.7424	1.7421	22.705	5.70	6.59	**23.9**	23.5
TR-18-09-2		342	198.026	83017004000	34.147	6.2635	59.388	16.70	19.06		
TR-18-09-3		262	204.919	35964684000	30.91	14.384	35.621	9.15	10.52		
TR-18-09-4		194	168.008	4741352000	25.284	7.5747	20.345	3.07	3.66		
TR-18-09-5		185	114.345	6798988000	11.006	6.7866	59.443	21.32	27.31		
TR-18-09-6		301	199.926	131792850000	41.178	13.288	60.726	23.71	27.16		
TR-18-09-7		201	113.476	19036444000	11.399	3.3926	109.34	57.12	72.65		

Table 3.3. Apatite-He dataset for Paintbrush Canyon

Paintbrush Canyon											
Sample	Elev (m)	Length (µm)	Width (µm)	He atoms	U (ppm)	Th (ppm)	Sm (ppm)	Raw Age	Corrected Age	Avg Age	Std Dev
TR-18-12-1	2527	181	151.024	1507408000	14.813	4.0174	43.622	2.22	2.7*	**7.7**	2.1
TR-18-12-2		238	229.989	5147100000	12.664	3.6813	56.325	2.88	3.28*		
TR-18-12-3		270	167.345	15606850000	18.993	7.6771	59.353	9.51	11.18*		
TR-18-12-4		174	147.895	4436138000	17.26	5.5083	87.555	5.99	7.33		
TR-18-12-6		157	113.813	3097892000	25.236	10.812	166.66	5.24	6.79		
TR-18-12-7		281	158.686	8151080000	18.862	5.2599	69.392	5.48	6.47		
TR-18-12-11		265	203.549	12390966000	13.695	44.222	70.633	4.47	5.19		
TR-18-12-12		278	180.051	20162786000	23.161	7.591	78.39	8.57	9.97		
TR-18-12-13		260	125.252	12911094000	30.627	10.136	118.47	9.18	11.32		
TR-18-12-14		195	136.715	6172306000	26.76	9.5463	108.71	5.58	6.87		

Table 3.4. Apatite-He dataset for Avalanche Canyon

Avalanche Canyon											
Sample	Elev (m)	Length (µm)	Width (µm)	He atoms	U (ppm)	Th (ppm)	Sm (ppm)	Raw Age	Corrected Age	Avg Age	Std Dev
TR-18-14-1	2298	227	135.996	18678254000	16.557	0.5466	64.294	25.44	31.02	**25.2**	5.0
TR-18-14-2		182	159.189	225705452000	13.819	0.1603	112.39	327.12	393.9*		
TR-18-14-3		234	146.67	20826792000	20.707	4.8092	51.968	18.16	21.88		
TR-18-14-4		287	193.915	785286726000	30.02	60.47	32.887	156.13	181*		
TR-18-14-5		296	163.044	93953538000	58.352	2.5904	109.39	19.42	22.79		
TR-18-14-6		171	124.061	842198000	32.385	3.0887	72.684	0.92	1.16*		

Table 3.5. Apatite-He dataset for Moran Canyon

Moran Canyon											
Sample	Elev (m)	Length (µm)	Width (µm)	He atoms	U (ppm)	Th (ppm)	Sm (ppm)	Raw Age	Corrected Age	Avg Age	Std Dev
TR-08-22-A	2188	101.2	63.5	4394600000	48.5	13.7	-	6.23	7.96	**8.0**	0.6
TR-08-22-B		143.8	56.4	6381200000	70.2	18.0	-	7.14	8.79		
TR-08-22-C		93.2	71.3	6321000000	79.4	25.2	-	6.17	7.84		
TR-08-22-D		101.2	76.4	8608600000	61.3	18.6	-	5.94	7.45		

3.2 Seismic interpretation and lake sediment volume calculations

Moran Bay, which is isolated from the rest of Jackson Lake by a large bedrock shoal (Figure 3.6), provides a unique opportunity to measure sediment volumes fluxed directly from the known catchment areas of Moran and Snowshoe Canyons. In the seismic reflection dataset of Moran Bay, key horizons interpreted to mark significant changes in depositional conditions (lake level, sediment supply, and fault motion) were mapped to provide a framework for measurement of sediment volumes. Because we do not currently have core data to establish absolute ages for each horizon, we have used stratal geometries and truncations of major reflectors to establish a relative depositional chronology for Horizons A through J (Figure 3.7). These horizons also allow us to build a stratigraphic framework for estimation of sediment accumulation rates, which can then be used to estimate denudation rates in Moran and Snowshoe Canyons.

The deepest horizon (A) interpreted in our processed seismic section is the top of the acoustic basement, a high amplitude reflector below which the seismic data yields no internal coherency. In a majority of cases (particularly in Moran Bay), this surface represents shallow bedrock or occurs at the base of thick sedimentary packages where i) bedrock may be present or ii) no more penetration is possible with our current imaging parameters. Above the acoustic basement are two potentially coeval packages exhibiting similar degrees of internal deformation and lack of coherency (Horizon B and B1) and truncating along the top of Horizon A (Figure 3.7). A package with distorted strata and nonuniform thickness (bound at its top by Horizon C) separates B and B1 from a laterally continuous package of consistent (isochoric) thickness with far less distortion (topped by Horizon D).

Above the isochoric package, we find evidence of significant progradation within Jackson Lake in a clinoform package (bound by Horizons D and E) with shelf margin geometry truncating along the top of Horizon D (Figure 3.7). Following deposition of this clinoformal package, a clear shift in depositional conditions occurred, possibly as a result of lake level increase or generation of accommodation space following a significant slip event along the Teton fault. This retrogradational package between Horizons E and F drapes over the clinoform package below (Horizon E) and out into the Moran Bay depocenter. This package also appears to be the youngest sediment package within Moran Bay that is either cut or distorted by the two inverted normal faults in the depocenter (Figure 3.7). Following deposition of Horizon F, lake level likely decreased once again, as we observe a series of stacked prograding clinoform packages (Horizons G, H) which feed sediment into the more distal portions of the bay and deposit it in uniformly thick, undeformed packages. Finally, in more recent periods of sedimentation in Moran Bay, it appears that the pace of sedimentation decreased, as evidenced by the final sediment package. The base of this package (Horizon I) truncates against the uppermost clinoform on the western portion of line D19 and lacks the central thickening present in lower packages. The sediment-water interface (Horizon J) marks the depth of modern sedimentation in Moran Bay. Thus, we have established an understanding of relative timing of changes in depositional conditions within Jackson Lake and can use this understanding to estimate denudation rates responsible for sedimentation between key horizons.

A total sediment thickness map for all of Jackson Lake was generated in Seisware by gridding Horizon A (acoustic basement) and Horizon J (waterbottom), depth converting both grids using a constant velocity model of 1500 m/s, and subtracting the depths of

Horizon J from those of Horizon A (Figure 3.8). This velocity model is based on the assumption that all imaged sediment is unconsolidated and waterlogged and thus possesses a similar seismic velocity to freshwater (Kindinger et al., 1994). In addition to the full lake sediment thickness map, isopach maps of Moran Bay total sediment and the more recent sediment above Horizon F were generated by clipping depth converted grids of Horizons A, F, and J to a Moran Bay shapefile and subtracting A-J and A-F (Figure 3.9). Using volumetric calculation tools in Trinity T3 software and these Moran Bay isopach maps, total bulk rock volume (BRV) within Moran Bay was determined to be 0.0074 km^3, with a maximum measured thickness of 24 meters over a data grid covering an area of ~2.22 km^2. Similarly, the BRV above Horizon F was 0.0047 km^3 with a maximum thickness of 12 meters. Such volumes represent a minimum estimate of all sediment that has entered Moran Bay (that can be imaged over the extent of our survey grid) if Moran Bay is topographically closed. However, if Moran Bay has an outlet into the main Jackson Lake depocenter that is not apparent in our survey (Figure 3.6), these volume estimates serve only as a preliminary estimate of total sediment flux into Moran Bay.

Though we do not yet have definitive age control of these mapped sediment packages, their distinct seismostratigraphic character allows us to calculate rates over a range of age possibilities, which will be discussed in greater detail in sections 4.1 and 4.2. As all Moran Bay sediment is assumed to be relatively young and unconsolidated, we apply porosity corrections to each BRV estimate according to

$$Eq.[2]\ \ Sediment\ volume\ (km^3) at\ low\ (30\%)\ \ porosity = BRV\ (km^3) * 0.7$$

$$Eq.[3]\ \ Sediment\ volume\ (km^3) at\ high\ (50\%)\ \ porosity = BRV (km^3) * 0.5$$

and present those results in Table 3.6.

Table 3.6. Volume Calculations of Key Sediment Packages

Sediment Package	Bulk Rock Volume (km^3)	Sediment Volume with Φ = 30% (km^3)	Sediment Volume with Φ = 50% (km^3)
Total Sediment (Horizon A-J)	0.0074	0.0052	0.0037
Holocene or Post-Dam (Horizon F-J)	0.0047	0.0033	0.0024

3.3 Calculation of denudation rates from lake sediment

In order to derive denudation rates from lake sediment volumes, a digital elevation model (DEM) was used in conjunction with ArcGIS hydrology tools to calculate the total catchment area of Moran and Snowshoe Canyons, as this is the area from which Moran Bay sediment was fluxed. Accounting for both Moran Canyon and Snowshoe Canyon drainages, we find a total catchment area of 70.88 km^2 that can supply sediment to Moran Bay (Figure 3.10). Using the porosity corrected volumes (results from Equations 2 and 3) and the catchment area, we use Equation 4 to calculate a basin-averaged denudation thickness for both the total and recent sediment packages.

$$Eq.\ [4]\ Denuded\ thickness\ (mm) = \frac{Porosity\ corrected\ volume\ (km^3)}{70.88\ km^2} * \frac{1{,}000{,}000\ mm}{km}$$

Then, we apply the two denudation possibilities (30% and 50% porosity) for each sediment package to the range of their age possibilities to derive basin-averaged denudation rates (Equation 5). We assume that Horizon A is likely a glacial scour surface, yielding age possibilities of 150 ka (Bull Lake scour) or 15.5 ka (Pd-2 scour). Because Horizon F potentially represents the boundary between glacial and postglacial sedimentation, its oldest likely age is 11.0 ka. As it may also represent the Dambrian surface, the youngest possibility for the age of Horizon F is 100 years. Assuming Horizon J is the modern sediment-water interface, we assign it an age of 0 Ma.

$$Eq.\ [5]\ Average\ denudation\ rate\ (mm\ yr^{-1}) = \frac{Denuded\ thickness\ (mm)}{Sediment\ package\ age\ (yrs)}$$

We find that the total sediment package (Horizon A-J) deposited due to a basin-averaged denudation rate of 0.00035 – 0.0047 mm yr^{-1}. Similarly, the younger sediment package above Horizon F is associated with denudation rates of 0.00303 – 0.4672 mm yr^{-1}. These ranges capture all denudation rate possibilities ranging from the low endmember case of i) high porosity sediment (low sediment volume) and ii) an old sediment package age (long period of denudation) to the upper endmember estimate of i) a low porosity (high sediment volume) and ii) young sediment package (shorter period of denudation). Results for each step of these calculations are outlined in Table 3.7.

Table 3.7. Apatite-He dataset for Paintbrush Canyon

Sediment Package	Volume with Φ = 30% (km^3)	Volume with Φ = 50% (km^3)	Total Catchment Area (km^2)	Oldest Age of Basal Horizon (yrs)	Youngest Age of Basal Horizon (yrs)	Basin-Averaged Denudation (mm/yr) (low porosity, old)	Basin-Averaged Denudation (mm/yr) (low porosity, young)	Basin-Averaged Denudation (mm/yr) (high porosity, old)	Basin-Averaged Denudation (mm/yr) (high porosity, young)
Total Sediment (Horizon A-J)	0.0052	0.0037	70.88	150000	15500	0.00049	0.00471	0.00035	0.00336
Holocene or Post-Dam (Horizon F-J)	0.0033	0.0024	70.88	11000	100	0.00425	0.46717	0.00303	0.33369

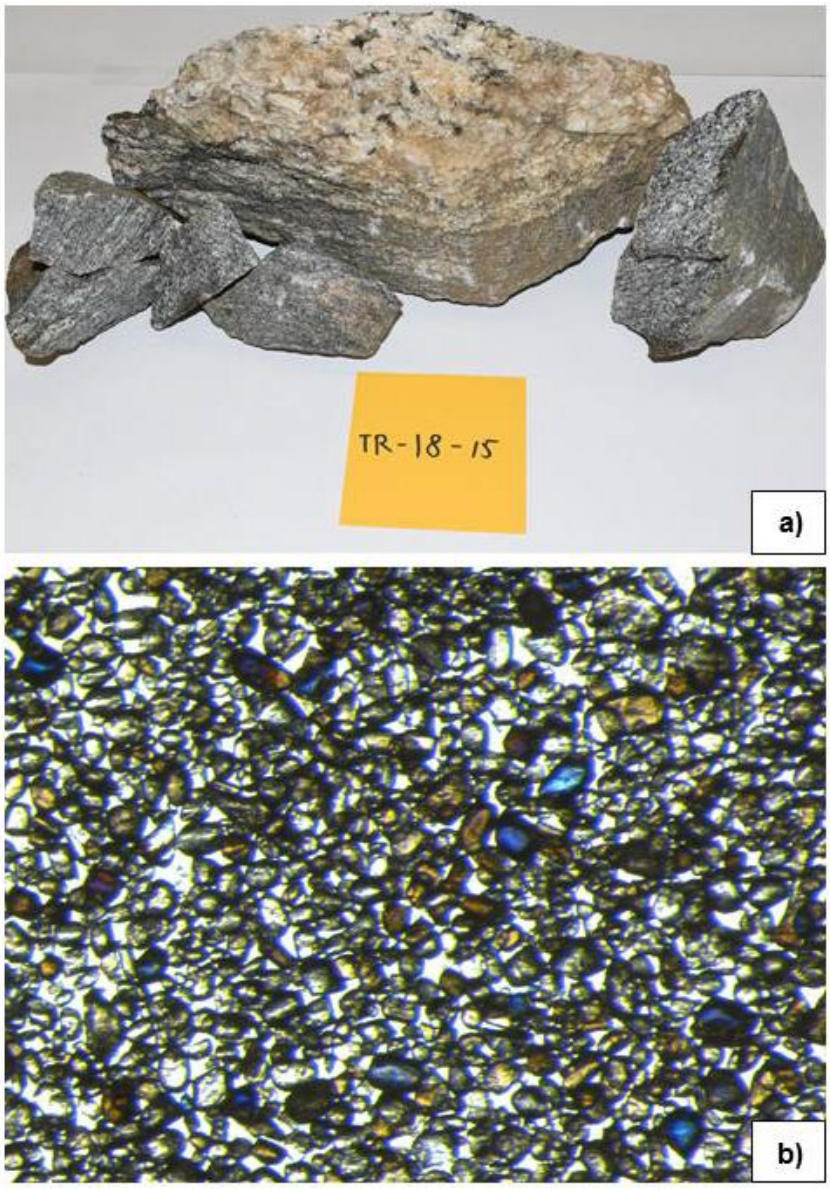

Figure 3.1- Death Canyon sample TR-18-15. Sample lithology is banded gneiss, though mapped as Mount Owen Quartz Monzonite (Love, 1992). Grains in separate are largely whole and heavily rounded. Many grains not selected due to abundance of large inclusions.

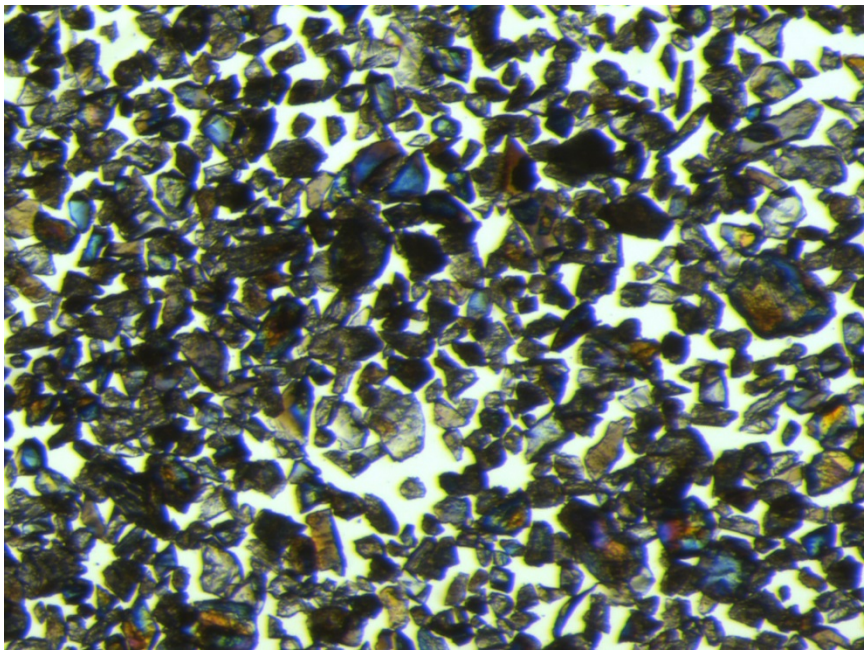

Figure 3.2 – Cascade Canyon sample TR-16-01. Apatite poor separate with heavily fractured grains due to diskmilling during sample processing. Lithology may not have been best suited for apatite abundance. Cascade Canyon samples will be recollected in future field seasons.

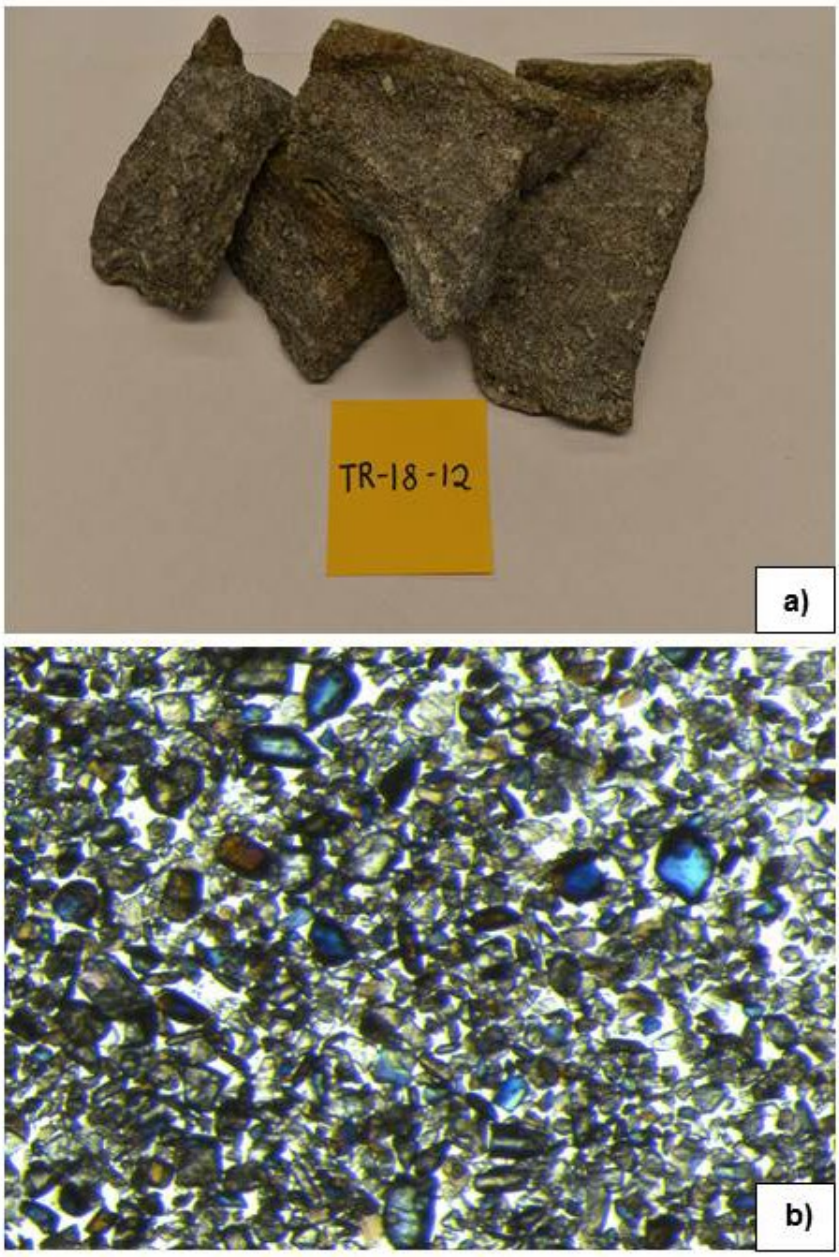

Figure 3.3 – Paintbrush Canyon sample TR-18-12 under cross-polarized light at 2.5 X. Sample contains abundant apatite with mostly euhedral grains. Original lithology more gneissic than other Paintbrush Canyon samples.

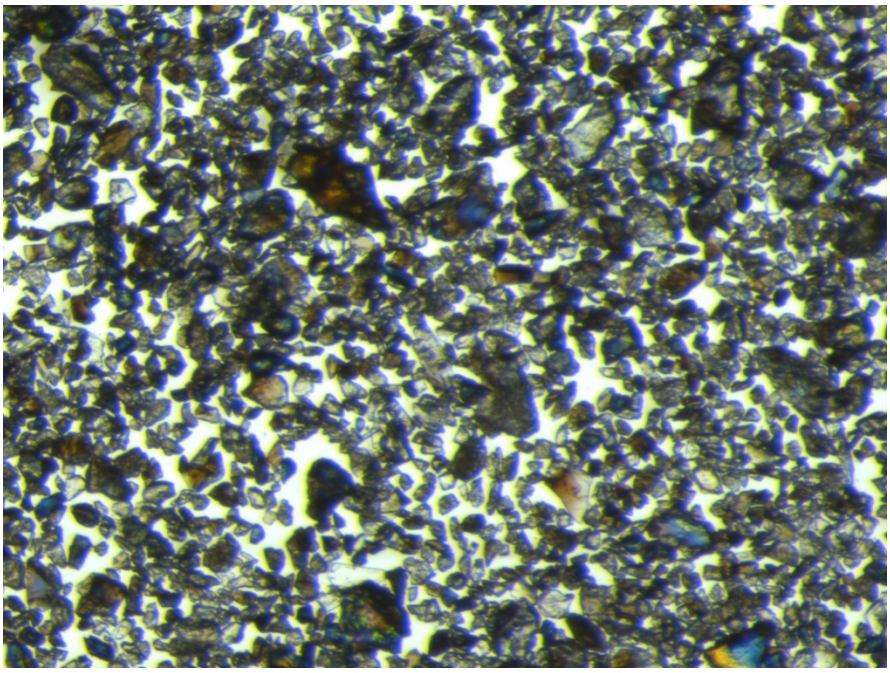

Figure 3.4 – TR-18-11 under cross-polarized light at 2.5 X. Sample is apatite poor and grains are much more heavily fractured than those of TR-18-12, despite being processed using the hammermill. No appropriate grains identified in this sample for AHe analysis.

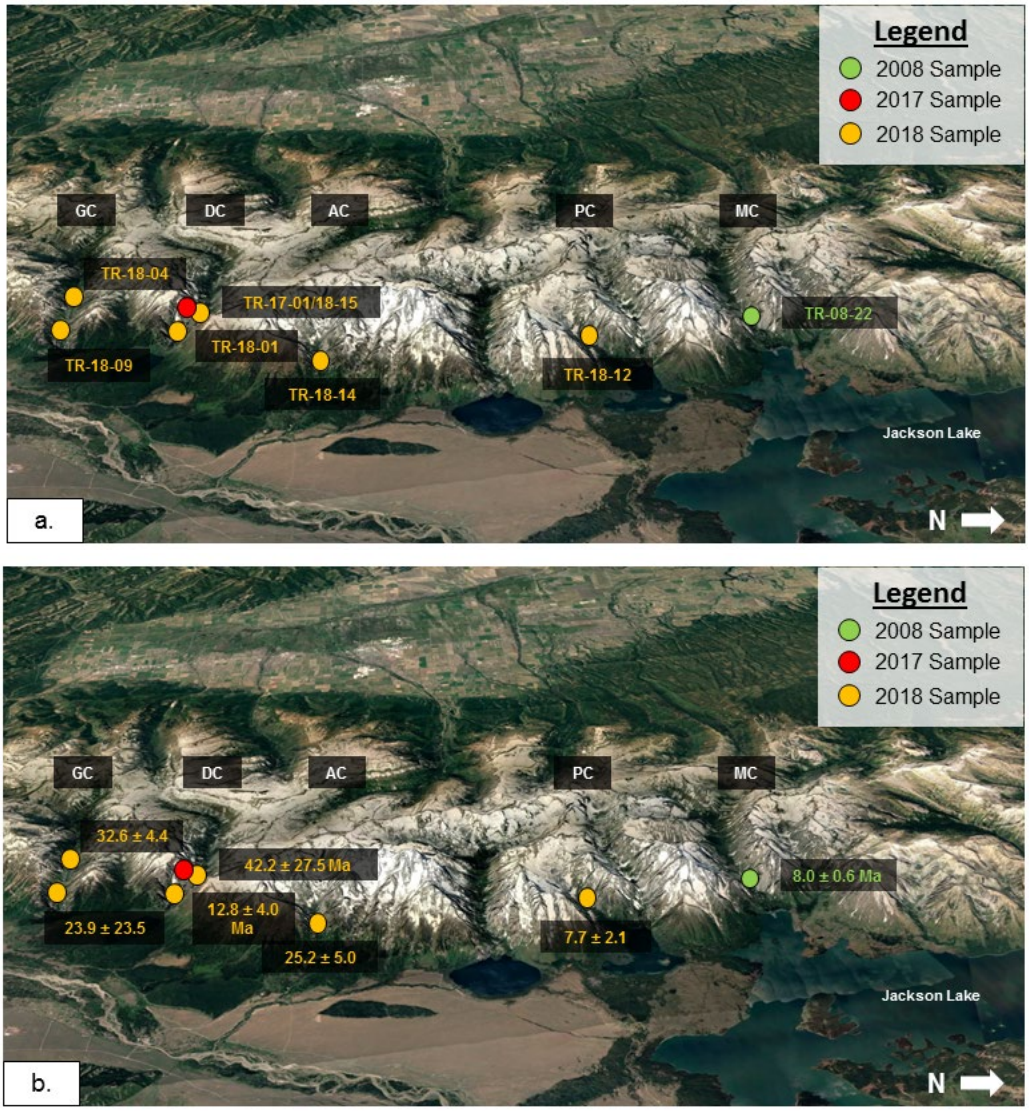

Figure 3.5 – a) eight samples with sufficient yield for AHe analysis and b) their average AHe age.

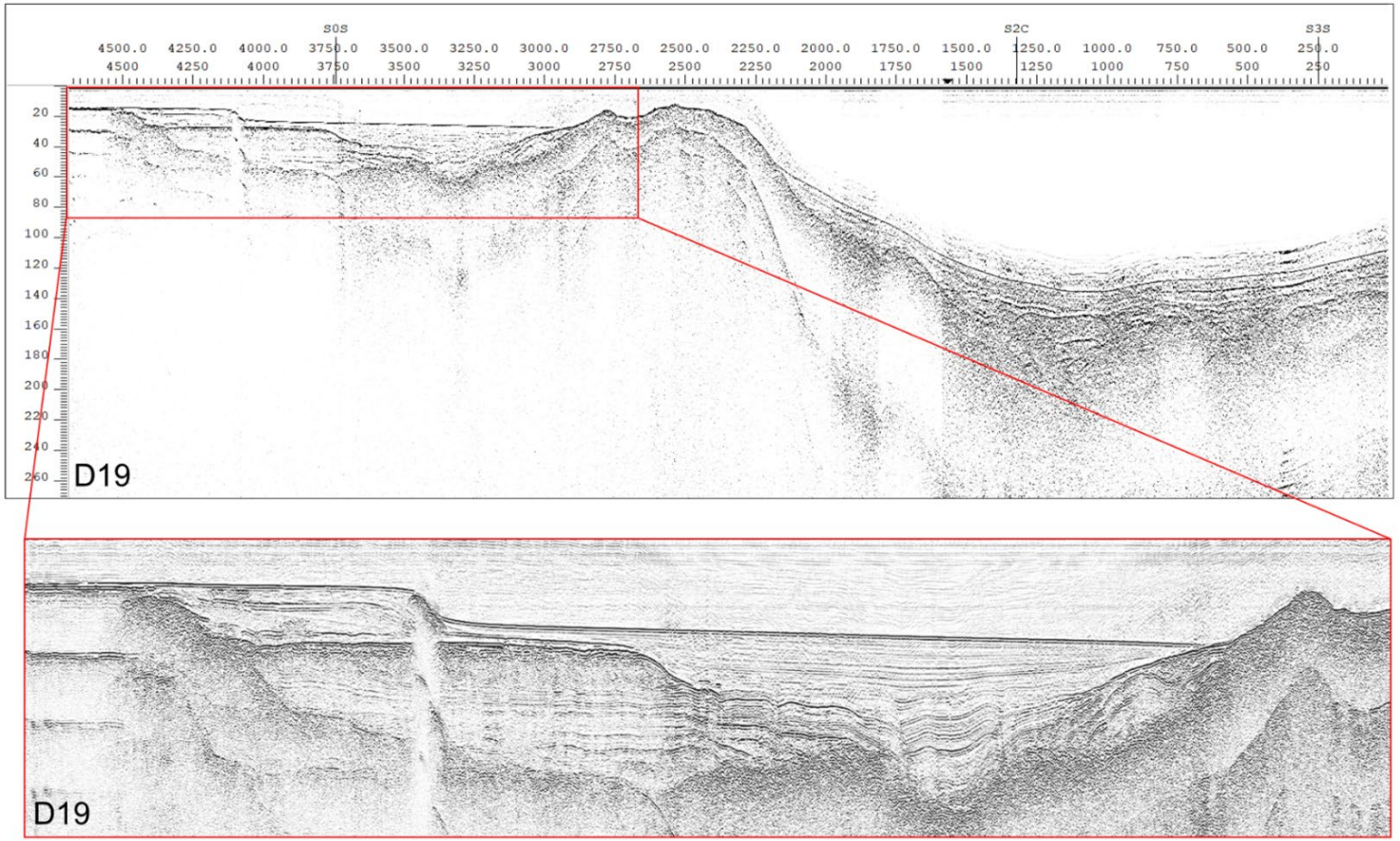

Figure 3.6 – CHIRP seismic line D19 with inset showing sediment deposited within Moran Canyon is isolated from the rest of Jackson Lake. Thus, we have a unique opportunity to measure discrete sediment volumes fluxed from the Moran Bay catchment.

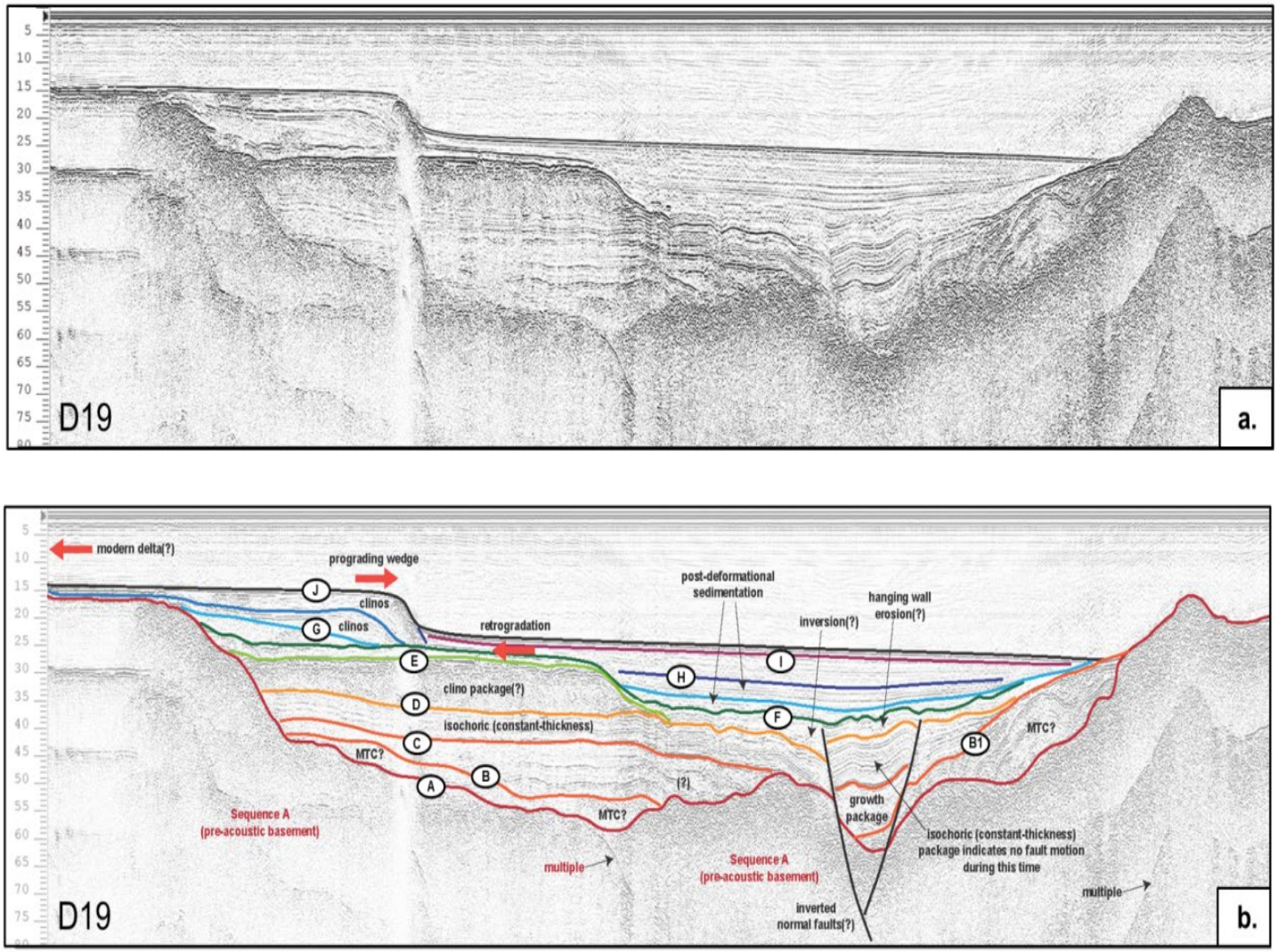

Figure 3.7 – CHIRP seismic line D19 showing mapped horizons.

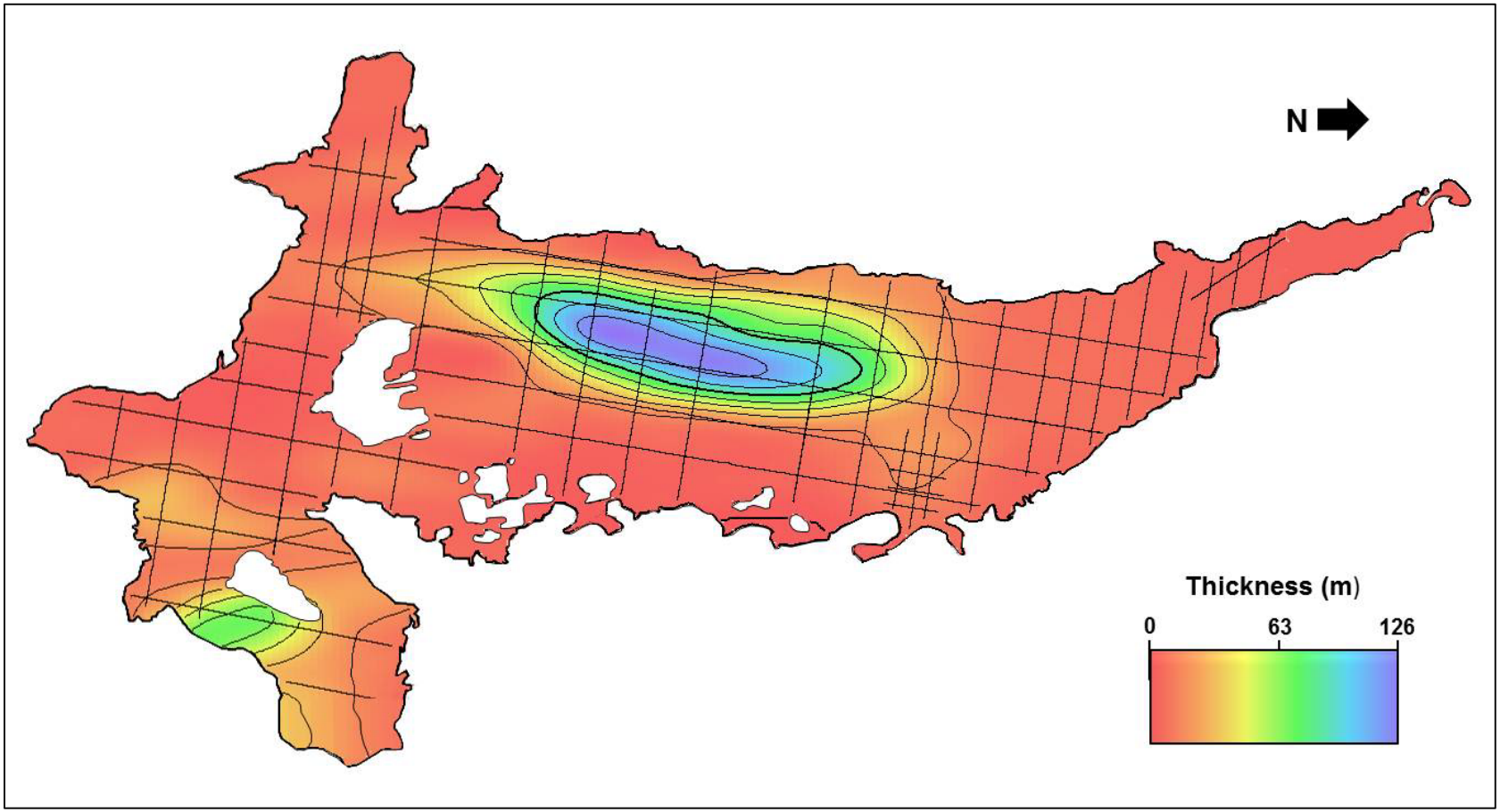

Figure 3.8 – Jackson Lake isopach map. Thicknesses calculated by depth converting grids in Seisware and subtracting lakewide waterbottom depths from acoustic basement depths.

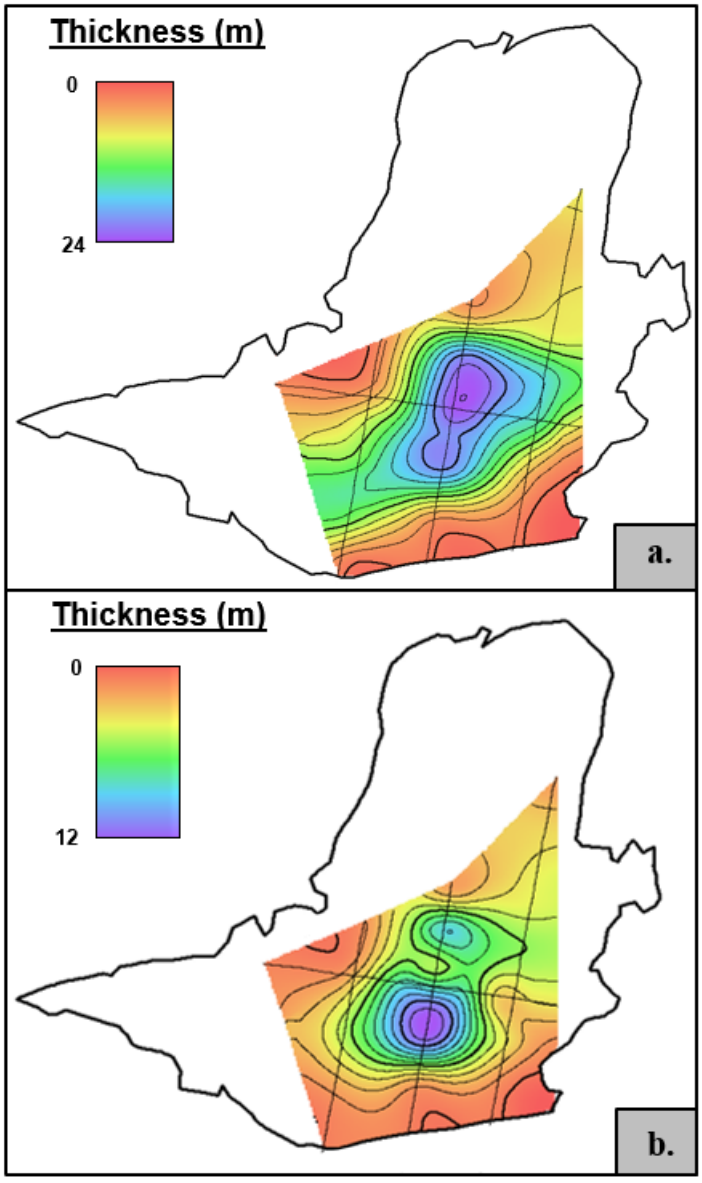

Figure 3.9 – Isopach maps of Moran Bay sediment volumes constrained by 2.22 km^2 seismic grid. a) Total sediment above acoustic basement (Horizon A-J). BRV = 0.0074 km^3. b) Sediment above candidate Dambrian/Holocene transitional surface (Horizon A-F). BRV = 0.0047 km^3.

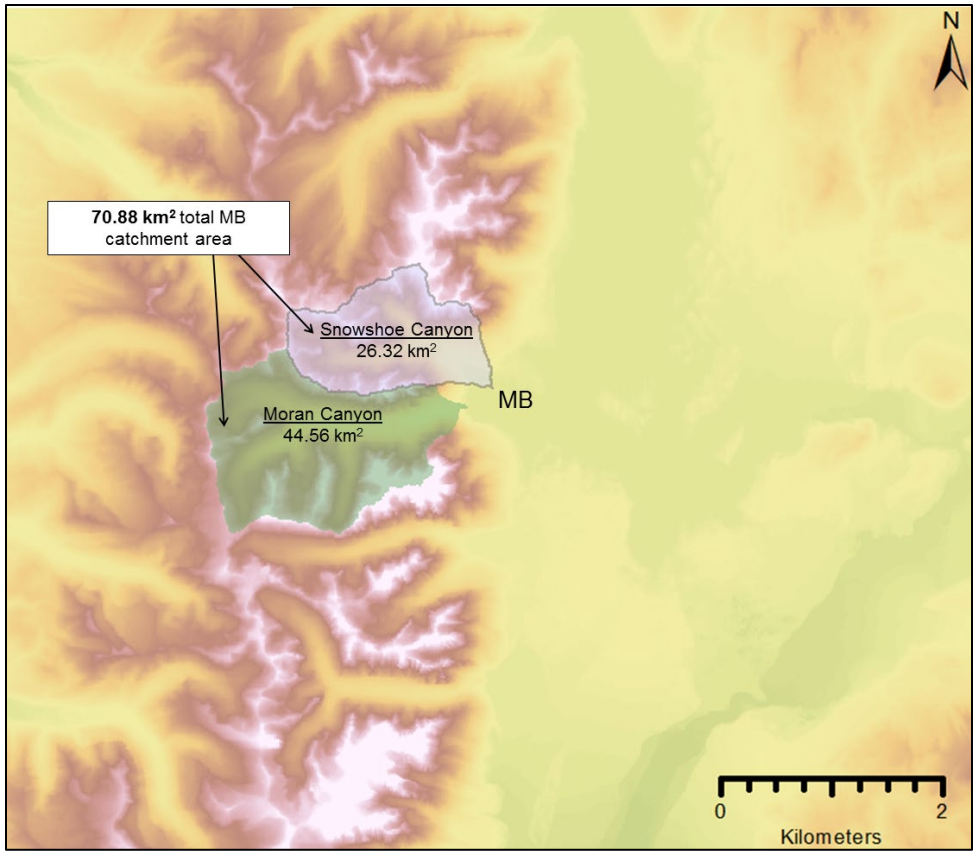

Figure 3.10 – Total catchment area of Moran Bay calculated from a Teton Range DEM. This total area was used in conjunction with sediment volume estimates to calculate basin-averaged denudation rates.

CHAPTER 4. DISCUSSION

4.1 Identifying distinct stratal packages and possible key age boundaries

In order to estimate denudation rates from the measured sediment volumes in Moran Bay, we use the relative chronology from our seismic data to determine a range of potential ages of key horizons that bound key stratal packages, as these ages represent the duration of denudation. Since we do not have age control from core in Jackson Lake at this time, the ages of Horizons A, F, and J are assumed to correspond to significant events in the Teton Range, which resulted in pronounced changes in depositional conditions. For example, we interpret Horizon A (acoustic basement) as a glacial scour surface because previous studies have shown that Jackson Lake was excavated by glaciers during both the Bull Lake and Pinedale glaciations (Pierce et al., 2018). Thus, a potential youngest age for the base of the sediment (Horizon A) is ~15.5 ka, or the $^{Be}10$ age of the Pd-2 terminal moraines on the southern end of the lake (Figure 1.3). Alternatively, the oldest possible age of Horizon A would correspond to the Bull Lake glaciation at ~150 ka. Though it is possible the acoustic basement (Horizon A) is not bedrock or a glacially scoured sediment surface, our estimated denudation rates for the Moran and Snowshoe watersheds that are calculated based on a presumed Moran Bay sediment age of 150-15.5 ka (0.00035 – 0.0047 mm yr^{-1}) likely encompasses the actual value.

Horizon F, regardless of its age, also represents a major change in depositional conditions within Moran Bay as it shows clear evidence for the onset of major retrogradation in Jackson Lake. Such retrogradation would be expected if deglaciation had recently begun. Further, packages deposited above Horizon F are most likely sourced from fluvial input on the western end of Moran Bay, as we observe the frequent buildup of

deltaic sand bodies in the shallower portions of our seismic section (Figure 3.7). Such deltaic sediment input would not be possible if sediment above Horizon F was deposited during a period of widespread glaciation with no fluvial activity in Moran and Snowshoe Canyon.

Further, Horizon F divides our imaged sediment package into two acoustically distinct packages. The package below Horizon F is distorted and faulted, with intermittent thickening and hummocky reflectors. Above Horizon F, however, the sediment assumes character much more typical of lacustrine sedimentation as opposed to glacial outwash deposits (e.g. Holocene diatom-rich muds, Larsen et al., 2016). Low reflectivity, highly continuous reflectors are present and there is essentially no internal distortion within these later packages. Previous work done at Jenny Lake (Larsen et al., 2016) found a similar distinction in acoustic character of a high-resolution seismic section, and core through this interval indicated that the upper boundary of the transitional interval between distorted, high reflectivity sediment and low reflectivity, uniform strata had an age of ~11.0 ka (Larsen et al., 2016). Thus, we propose that Horizon F in our section may represent the glacial-postglacial transitional surface (11.0 ka). If Horizon F has an age of ~11.0 ka that would yield watershed averaged denudation rates of 0.0030 – 0.0043 mm yr^{-1}.

Alternatively, it is possible that Horizon F corresponds to a fundamental change in depositional conditions following emplacement of Jackson Dam in 1911. This possibility is supported primarily by a difference in two way travel time (~10 ms) between Horizons F and J that, when depth converted, suggests a lake level increase similar to the 7.5 m increase measured between 1909 and 2018 (Figure 2.4). In this scenario, Horizon F would have an age of ~100 years. If Horizon F is ~100 yrs old, calculated basin-averaged

denudation rates in the Moran and Snowshoe watersheds would be ~0.4672 mm yr^{-1} based on the volume of sediment deposited above Horizon F.

Still another possibility is that Horizon J, rather than having an age of 0 years, could potentially be the 100 year old "Dambrian" surface. Its geometry is indicative of retrogradation, and aerial imagery indicates that the modern Moran and Snowshoe deltas are much further to the west than westernmost extent of line D19 (Figures 3.7 and 4.1). Additionally, clinoform packages G and H are likely paleo features since the topset- foreset transition (Figure 3.7) is lower than the modern lake level. This suggests that modern deltaic sedimentation is occurring further to the west and Horizon J may have an age of ~100 years. Further CHIRP surveying closer to the mouth of Moran Canyon may be necessary to image the true modern delta and corroborate this interpretation. If indeed Horizon J is the Dambrian surface, the denudation rate estimate for the recent sediment package assuming a basal age of 11.0 ka would increase, as 100 years of erosion time would effectively be removed. As there is evidence for multiple age scenarios of our most key seismic horizons, it will be necessary in future field seasons to acquire long sediment cores through key portions of the seismic section (Figure 4.2) to provide age control of Horizons A, F, and J and refine denudation rate estimates accordingly.

4.2 Determining short-term denudation rates from sediment volumes

In Moran Bay, we determined that the minimum estimate of total sediment flux from the Moran and Snowshoe Canyon watersheds is ~0.007 km^3. This estimate includes all sediment currently imaged in Moran Bay above the acoustic basement Horizon A, though serves as a minimum estimate of sediment thickness due to the limited seismic coverage of Moran Bay in its entirety (Figure 3.9). When corrected for a range of potential porosity

values (30-50%), the volume of sediment is calculated to range between 0.0037 and 0.0052 km^3. Further, above Horizon F, we find a sediment volume of 0.0047 km^3. Applying the same porosity correction yields a range of 0.0024 – 0.0033 km^3 of more recently deposited Moran Bay sediment.

Denudation rates using the total sediment volume in Moran Bay were calculated to be 0.00049 – 0.0047 mm yr^{-1} assuming low porosity (Φ = 30%). For the high porosity case (Φ = 50%), denudation rates over the timescale of deposition of this package range from 0.00035 – 0.0034 mm yr^{-1}. For the more recent sediment package (above Horizon F), these low and high porosity denudation estimates are 0.00425 – 0.4672 mm yr^{-1} and 0.00303 – 0.33369 mm yr^{-1}, respectively. Tranel et al (2015) calculated a spatially averaged rate across four Teton canyons of 0.2 mm yr^{-1}, which falls comfortably within our estimated range using the recent lake sediment. Additionally, Tranel et al. (2011) used detrital AHe methods to derive basin-averaged denudation rates in Garnet Canyon alone. Resulting estimates of 0.16 - 0.27 mm yr^{-1} agree similarly with our recent lake sediment estimates. Further, our seismic survey did not cover the entirety of Moran Bay, so all denudation rates derived from sediment volumes are a minimum estimate. Were a higher density, larger survey grid collected in future field seasons, it is likely that resulting denudation rates would be more similar to those of other studies.

Though we are confident that rate estimates derived from lake sediment volumes capture a reasonable range of true rates over postglacial timescales, when examining denudation rates it is important to also consider volumes of sediment that have been eroded but not yet deposited in Jackson Lake. National Park Service LiDAR data provides a means of estimating such stored sediment in Avalanche and Moran Canyons (Figure 4.3). In a

previous study, Johnson et al. (2019) measured talus and debris volumes over an area of 5.07 km^2 in Moran Canyon of 0.089 km^3, whereas in Avalanche Canyon that same study calculated talus volumes of 0.023 km^3 over an area of 1.3 km^2.

If it is assumed that these volumes of talus and sediment were produced following the final phase of Pinedale scouring, it is possible to use Equations 4 and 5 to estimate basin-averaged denudation rates on the post-glacial timescale (15.5 ka) of 1.13 and 1.14 mm yr^{-1} in Moran and Avalanche Canyons, respectively (Table 4.1). These rates are notably higher than any of the denudation rates calculated by this study from the Moran Bay sediment volumes, and agree relatively well with similar work done by Tranel et al (2015). In that study, talus volumes measured in four Teton Range catchments (Avalanche, Garnet, and Cascade Canyons, and Glacier Gulch) indicated that short-term rock fall rates are roughly 0.8 mm yr^{-1}. Such rates were consistent regardless of catchment size, similar to our findings within Moran and Avalanche Canyons. Modeling work has also been done by Foster et al. (2008, 2010) to derive short-term rock fall rates of 0.5 -1.0 mm yr^{-1}, similar once again in magnitude to the estimates for Avalanche and Moran Canyons (Johnson et al., 2019).

Small volumes of Moran Bay sediment, particularly above Horizon F, appear to be more fluvially sourced than the older sediment. Clinoform packages G and H in particular suggest the buildup of prograding sands at the mouth of a river exiting Moran Canyon. The low denudation rates derived from these sediment volumes suggest that, if fluvial transport is a significant mechanism for Moran Bay sedimentation, it is responsible for comparatively little mass efflux in the Teton Range as a whole. It is more likely that a majority of sediment transport is ultimately accomplished during periods of glacial activity.

Therefore, we conclude that large volumes of stored sediment and talus present in Teton Range canyons will not be easily transported into glacial range-front lakes until the next period of glacial advance.

Table 4.1. Denudation Rate Calculations Using Canyon Sediment

Canyon	Area of Measurement (km^2)	Stored Sediment Volume (km^3)	Duration of Denudation (yrs)	Area-Averaged Denudation Rate (mm/yr)
Moran	5.07	0.089	15,500	1.13
Avalanche	1.3	0.023	15,500	1.14

4.3 Long-term incision rates from thermochronologic results

Though many bedrock samples yield AHe ages that are older than the age of fault slip onset as determined from inverse thermal history modeling (e.g., Brown et al. 2017; Hoar, 2019), both Paintbrush and Moran Canyon (TR-18-12, TR-08-22) yield AHe ages that are younger than fault slip onset in that region. Because of this, it is possible to estimate long-term incision rates for these canyons by dividing total exhumation by the lag time between fault slip onset (13 Ma) and the canyon sample age.

$$Eq.\ [6]: \frac{Paleo\ PRZ\ elevation\ (m) - Sample\ elevation\ (m)}{(slip\ onset\ age\ (Ma) - sample\ age\ (Ma)}$$

Paintbrush Canyon yields an average AHe age of 7.7 ± 2.1 Ma (*n=7*), whereas Moran Canyon yields an average AHe age of 8.0 ± 0.6 Ma (*n=4*). Such reliable ages, when compared to the nearest slip onset age at Mount Moran (13 Ma), reveal that this portion of the range is where the most rapid denudation is occurring. From time of slip onset at 13 Ma, Paintbrush Canyon incised 173 m (from paleo-PRZ projected elevation of 2700 m to TR-18-12 elevation of 2527 m), indicating an estimated long-term incision rate of 0.03 mm/yr. Moran Canyon has a total age lag of 5 Ma, leading to a calculated incision rate of ~0.24 mm/yr. Further, because Mount Moran yields the youngest age of slip onset and the greatest magnitude of measured slip, Brown et al. (2017) interpreted the Moran region to represent the approximate center of the Teton fault. However, as the Grand Teton currently has the highest elevation point in the range but has a slip onset age of 10 Ma, we propose that increased denudation in the northern portion of the range in response to more rapid uplift potentially contributes to Mount Moran not being the highest Teton Range peak. Further, Foster et al. (2010) suggests that the closer spacing of cirques near Mount Moran contributes to greater lateral erosion and lower resulting elevation compared to Grand

Teton. Finally, the sustained high elevations and hillslope gradients of Grand Teton and Mount Moran are likely a function of their tendency to behave as "Teflon peaks" (Foster et al., 2008). Composed of the most resistant crystalline basement units at the core of the range, these peaks appear to be the only exception in the range to the efficacy of the "glacial buzzsaw." Overall, calculated long-term incision rates agree quite well with the 0.14 mm yr^{-1} rate estimated previously (Brown et al., 2017), and we propose that rates decrease as distance from the Mount Moran transect increases. This is further supported by generating age-elevation gradients for the entire Teton Range AHe dataset (Figure 4.5). We find that gradient decreases systematically from north to south, suggesting that samples in the south must be collected from comparatively low elevations in order for the apatite grains to yield reset ages.

4.4 Comparison of short and long-term denudation rates

Based on the results of this study and previous works, it is clear that denudation rates measured in different parts of the Teton Range over vary significantly in magnitude. We find long-term incision rates derived from canyon AHe ages scale logically with uplift rate and magnitude determined by Brown et al. (2017). That is, the segments of the range that have experienced the most substantial exhumation over the last 13 Myr also yield the highest incision rates. Long-term incision rates (e.g. 0.24 mm yr^{-1}) also agree well with the previously determined range-wide average denudation rates of 0.14 mm yr^{-1} determined by Brown et al. (2017) using large scale volumetric reconstructions. Over postglacial timescales, we find that short-term rock fall rates in Teton Range canyons are an order of magnitude higher than the long-term incision rates (1.14 vs. 0.24 mm yr^{-1}).

Finally, we present basin-averaged denudation rate estimates derived from lake sediment packages preserved in Moran Bay. These estimates depend heavily upon the ages of key seismic horizons, but we find that, logically, the most recent sediment package in Moran Bay (above Horizon F) is associated with basin-averaged denudation rates similar to recent estimates derived by other studies (Tranel et al., 2011, 2015). Thus, long-term denudation rates in the Teton Range seem to scale appropriately with tectonic forcing while shorter-term rates as measured by stored canyon sediment can be far higher (1.13-1.14 mm yr^{-1}) while shorter-term rates derived from lake sediment volumes are much lower.

4.5 Implications of variability in multitemporal rates for denudation mechanics

Much work has been done in tectonically active systems to determine how mountain systems erode (Willett, 1999; Konstantinovskaia and Malavieille, 2005; Godard et al., 2006; Whipple, 2009; Roe and Brandon, 2011). We find that over short timescales, extreme (1.13-1.14 mm yr^{-1}) denudation rates are possible when they result from high-energy, stochastic canyon processes such as rockfall and landslide events. Rockfall rates derived from the volume of canyon talus deposits agree with those in other studies regardless of along-strike position. This suggests that in the short-term, mass wasting rates are independent of tectonic forcing, as this is known to vary significantly across the Teton Range.

Overall, however, we propose that tectonic uplift seems to dictate denudation rates when averaged over Myr timescales and multiple glacial-interglacial cycles as AHe-derived incision rates are highest in areas of greatest uplift. Currently we find that the total volume of sediment in Moran Bay (0.007 km^3) is roughly an order of magnitude lower than

the volume of post-glacial talus present in just a small portion of Moran Canyon (0.089 km^3). Thus, we propose that the Teton system is transport limited in the interglacial, as the short-lived fluvial networks currently present are far weaker erosional agents than advancing valley glaciers. This supports the conclusions of Koppes and Montgomery (2009), who propose that fluvial and glacial erosion are capable of similar volumes of erosion, but only where the active system is of a sufficient size to sustain high-energy fluvial processes through time. In small systems such as the Teton Range where this is not possible, the vast majority of efflux is attributed to punctuated periods of glacial activity.

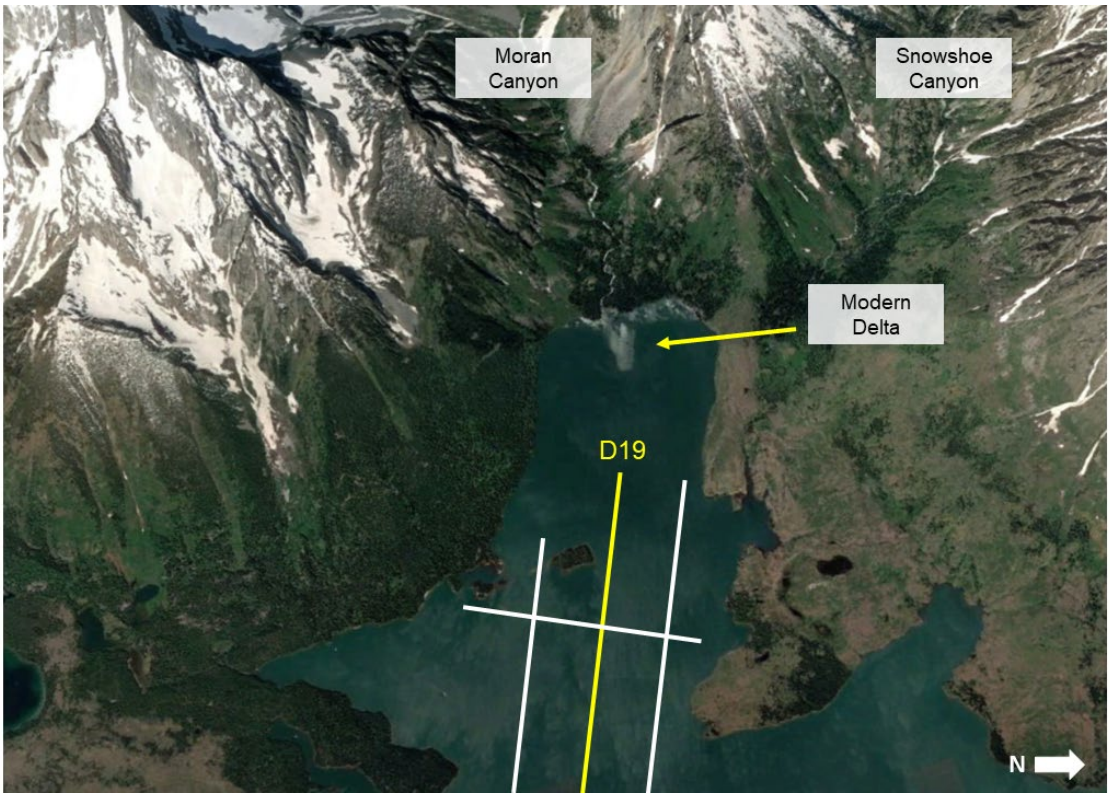

Figure 4.1 – Google Earth imagery showing modern deltaic sediment accumulation at mouth of Moran Canyon, well outside the extent of our current seismic survey. We propose this as evidence that Horizon J (Figure 3.7) may represent the Dambrian surface and the surface representing current sediment accumulation is not imaged.

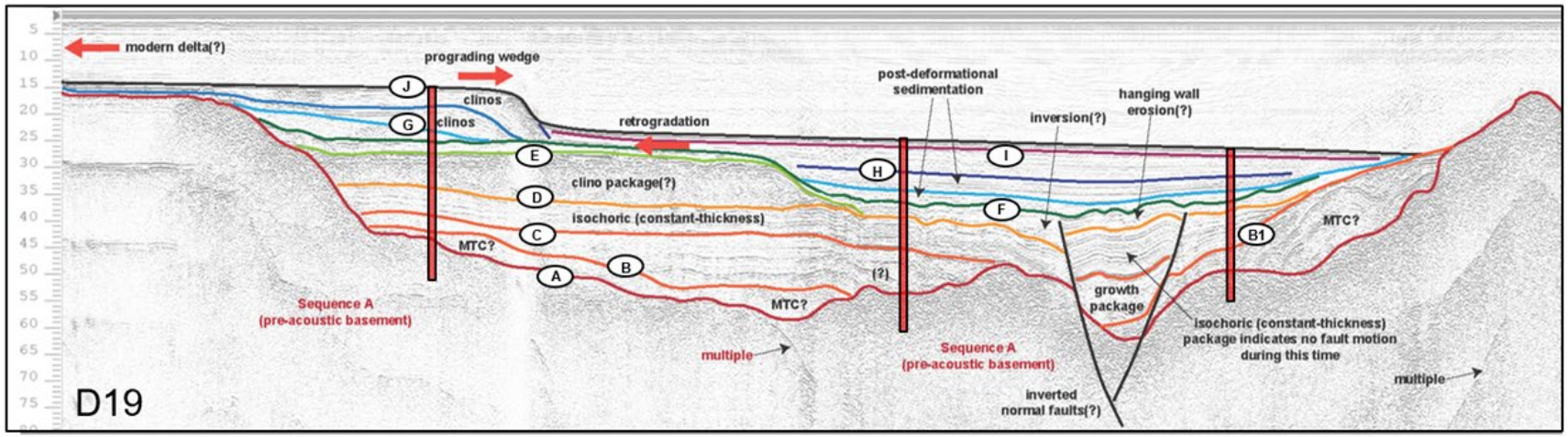

Figure 4.2 – Proposed coring targets penetrating key seismic horizons for age control and refinement of lake sediment derived denudation rate estimates.

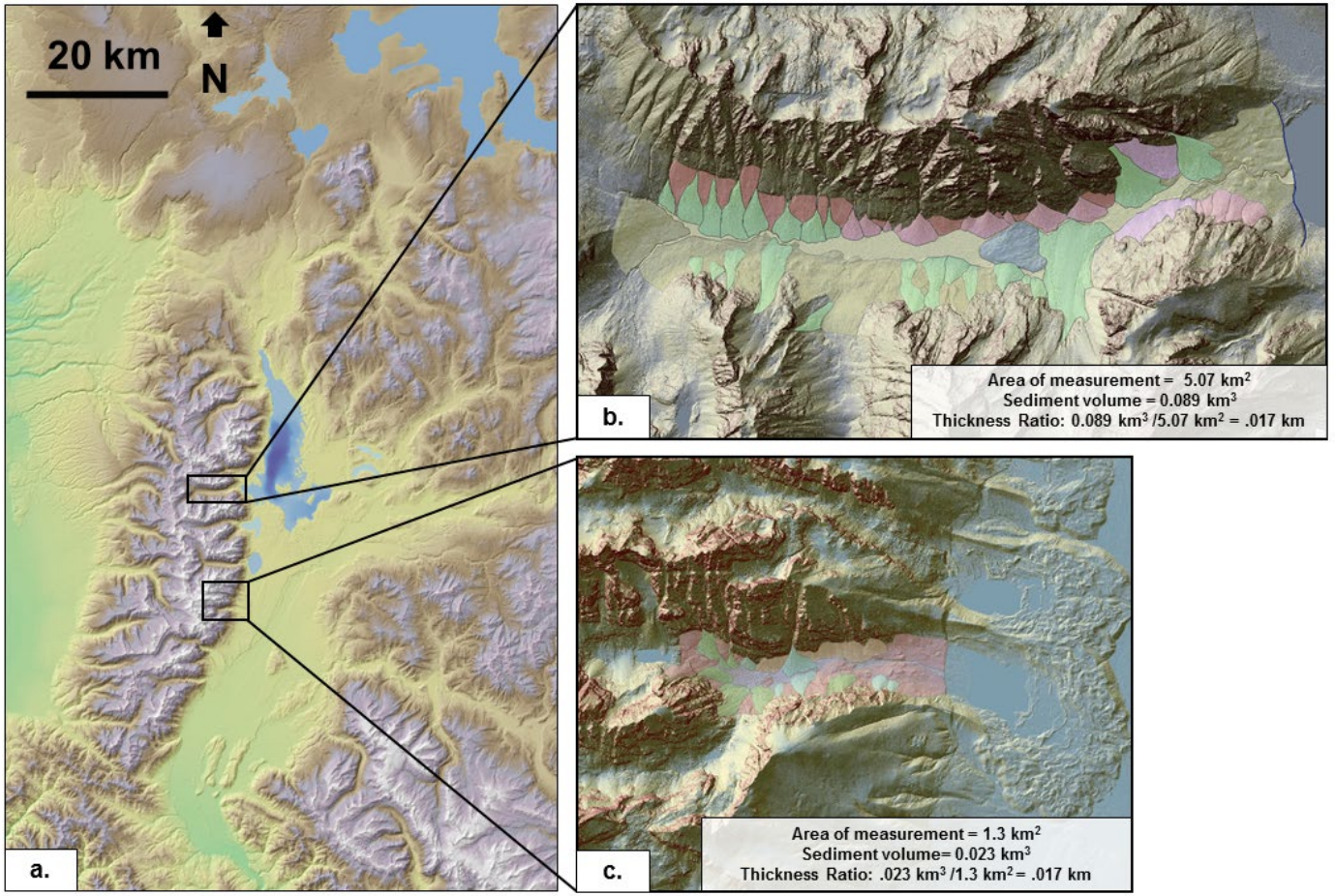

Figure 4.3 – Stored sediment measurements using LiDAR data. a) Teton Range with location of Moran and Avalanche Canyons. b) Moran Canyon LiDAR with mapped deposits and total sediment volume of .089 km^3. c) Avalanche Canyon LiDAR and stored sediment measurement of .023 km^3.

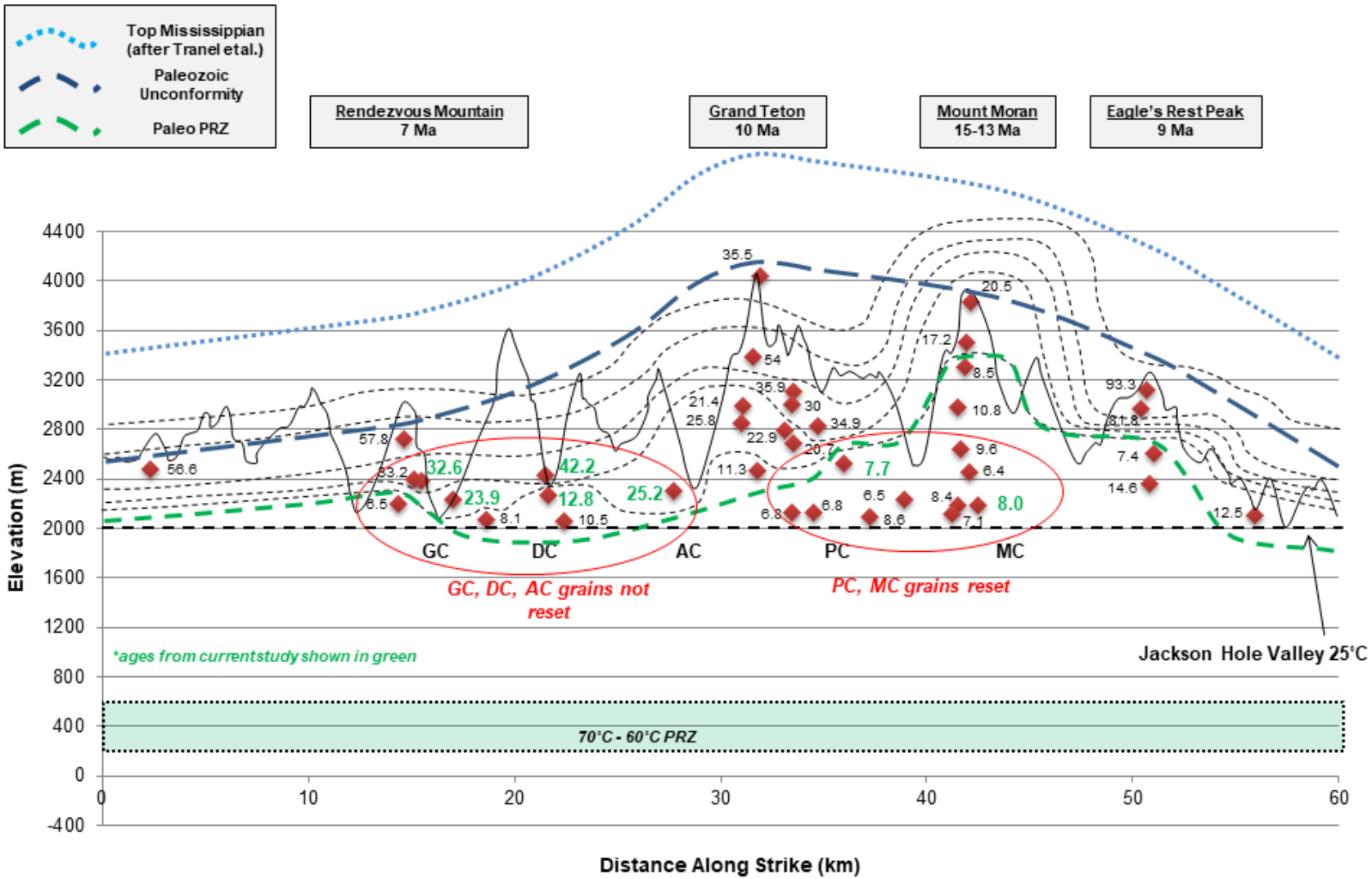

Figure 4.4 – Synoptic figure of AHe ages along strike.

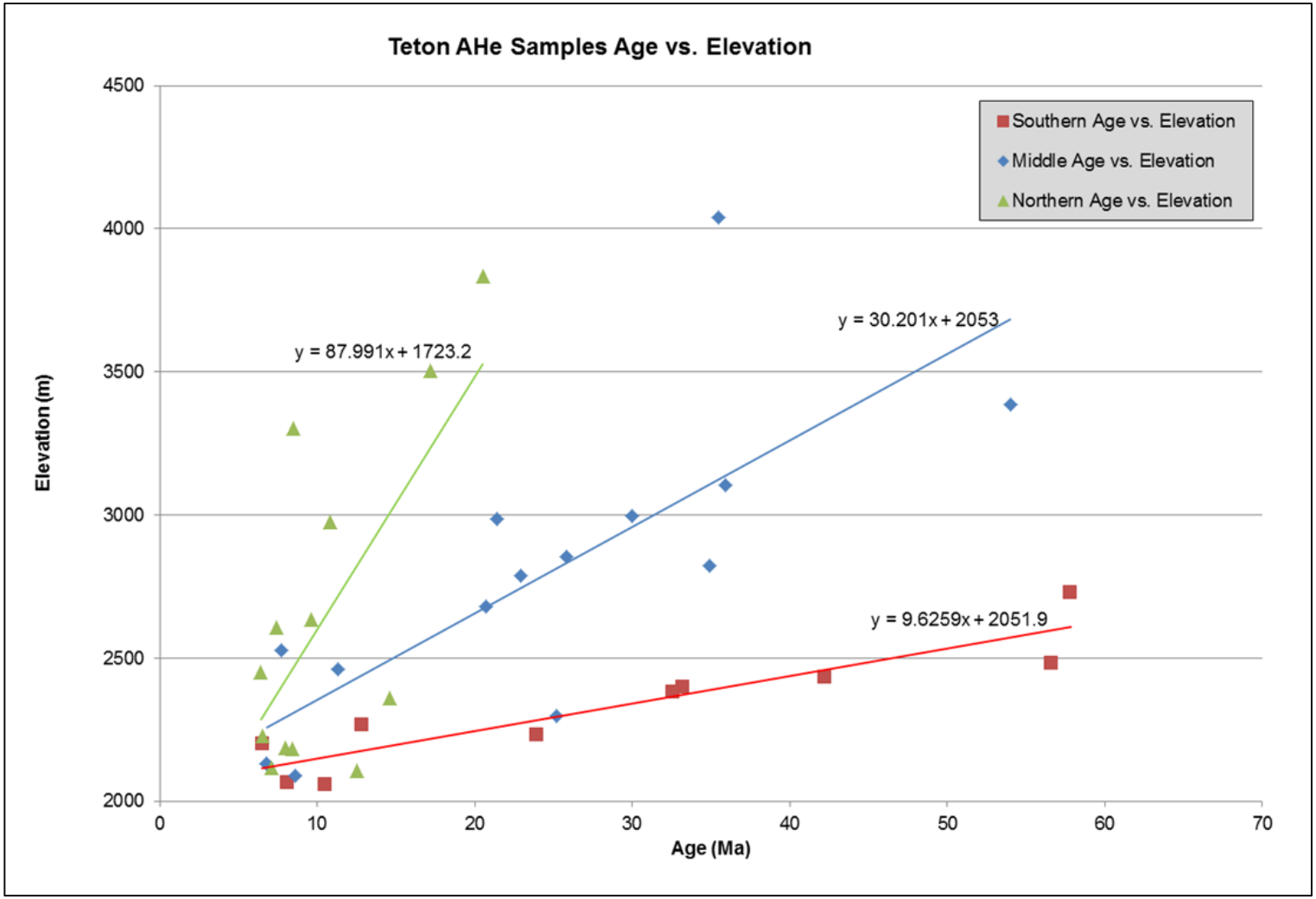

Figure 4.5 – Teton Range age-elevation gradients for all AHe samples to date. Gradient decreases from N-S with uplift variation. Suggests covariation between uplift and exhumation rates.

CHAPTER 5. CONCLUSIONS AND FUTURE WORK

5.1 Key study findings

In this study we address the longstanding challenge of determining what factors govern mountain denudation rates in active systems. We take a multitemporal approach, using AHe thermochronology to derive long-term incision rates and seismic surveying of Jackson Lake to derive short-term denudation rates.

Through the thermochronology portion of this study, we conclude that long-term incision rates in the Teton Range are ultimately a function of rock uplift rates, as our calculated incision rates are highest in the areas where the most exhumation has occurred (e.g. nearest to Mount Moran). In fact, where total uplift has been slower and occurred to a lesser degree in the southern portion of the range (e.g. Rendezvous Mountain), we do not find apatite grains with reset AHe ages, suggesting that insufficient incision has occurred in these areas to expose the Paleo-PRZ for sampling.

On shorter timescales, we find that extremely high rock fall rates (1.13-1.14 mm yr^{-1}) are possible in canyons across the range (and in other canyons from Tranel et al., 2015). This suggests that stochastic mass wasting processes during interglacial periods are not a first-order function of along strike variability in uplift rates. Despite their magnitude, such high rates of mass wasting are not sustained over long periods of time, as lake sediment volumes are associated with denudation rates a full order of magnitude lower. Finally, we conclude that, consistent with the findings of Koppes and Montgomery (2009), small mountain ranges such as the Tetons are not capable of removing large volumes of material from fluvial processes alone, despite the erosive capabilities of fluvial systems in larger orogens such as the Himalaya. Because the Tetons are in an interglacial period, key

catchments such as Moran and Snowshoe Canyons are experiencing massive rock fall denudation rates, but this talus and debris is not advected to Moran Bay in the absence of advancing valley glaciers.

5.2 Knowledge gaps and future work

In upcoming field seasons, a primary objective is to complete the canyon transects that were not performed in 2016, 2017, or 2018 to fill in the along-strike dataset of long-term incision rates. One of the key canyons lying in similar along-strike positions to the Mount Moran subvertical transect is Leigh Canyon. This canyon is untrailed and lies in grizzly bear territory, thus it has not been sampled yet due to ease and safety of access. AHe age results from this canyon would be beneficial for comparison of the long-term canyon incision rates with those of the shorter term sediment flux rates into Moran Bay, and would complement the age of 8.0 ± 0.6 Ma from Moran Canyon and 7.7 ± 2.1 Ma from Paintbrush Canyon which can be compared to the Mount Moran slip onset time (13 Ma).

Additionally, samples that did not give adequate apatite yields for AHe analysis in this study should be recollected with particular regard for lithology wherever possible. From this study, we found that banded gneisses and quartz monzonites provide more reliable yield than the felsic granites. Transects of Cascade and Webb Canyons should be repeated to replace samples TR-16-01, TR-16-02, and TR-16-03 (Figure 5.1).

Of additional importance for improving the estimates of shorter-term denudation rates is definitive age control within Moran Bay sediment packages. We recommend collecting several long sediment cores in key areas of Jackson Lake, including Moran Bay (Figure 4.2) and each of the major depocenters (Figure 5.2). Age control and porosity measurements cores will enable more refined measurements of total sediment volume and

improved denudation rate calculations. Further, as all denudation rate estimates in this study are derived from minimum sediment volume estimates, more robust seismic coverage of Moran Bay could also improve these calculations.

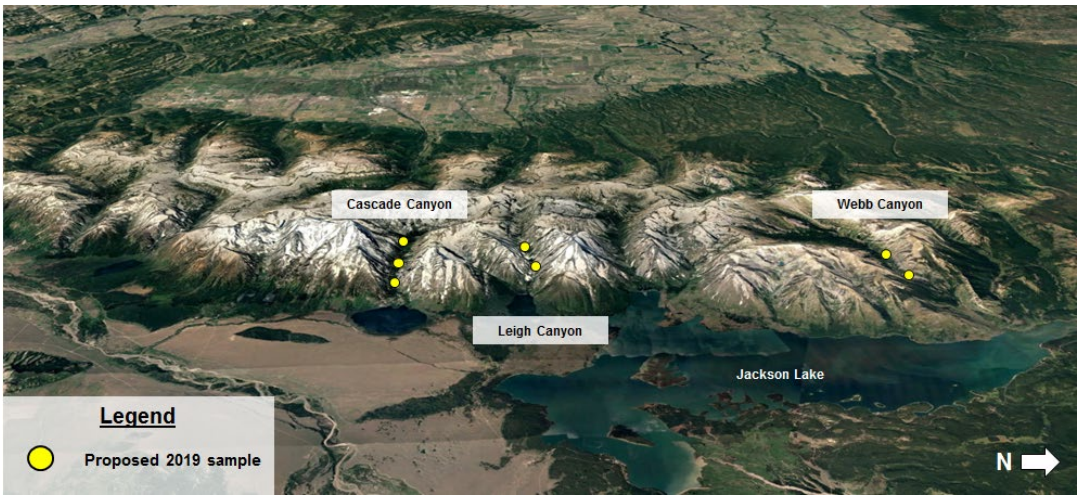

Figure 5.1 Proposed future canyon samples from Cascade, Leigh, and Webb Canyons. Cascade and Webb Canyons to be resampled at increased density due to yield quality in 2016-2018 samples. Leigh Canyon to be sampled for the first time.

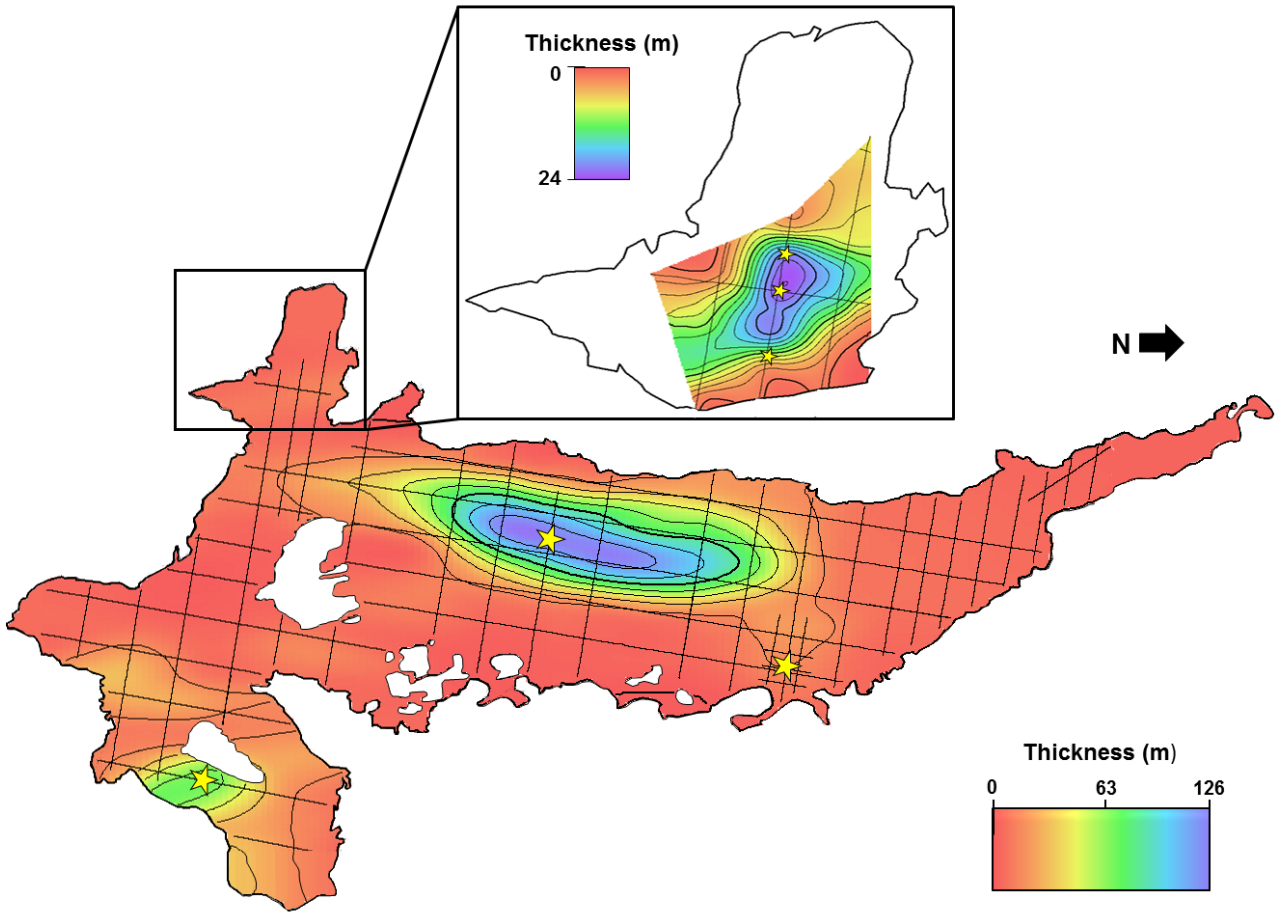

Figure 5.2 – Coring targets for summer 2019 field campaign on sediment thickness map of Jackson Lake.

Coring targets all selected based upon potential for penetrating seismic horizons for age control.

APPENDIX

APATITE GRAIN PHOTOS AND MEASUREMENTS

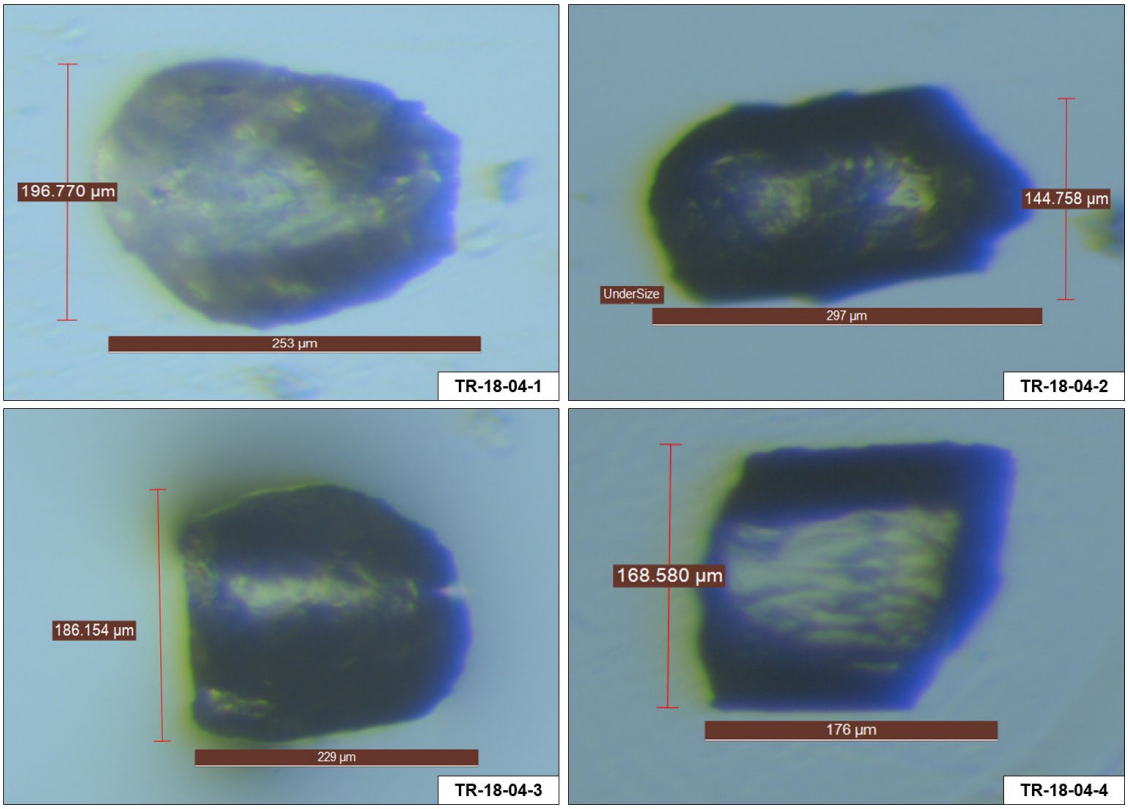

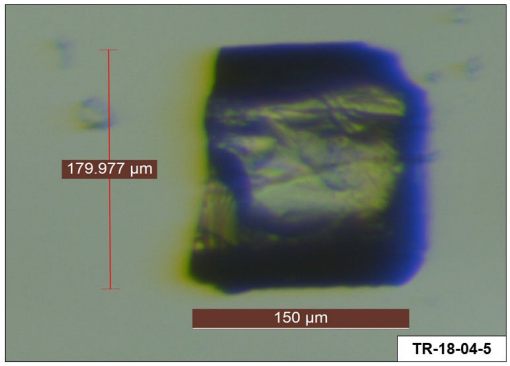
179.977 µm
150 µm
TR-18-04-5

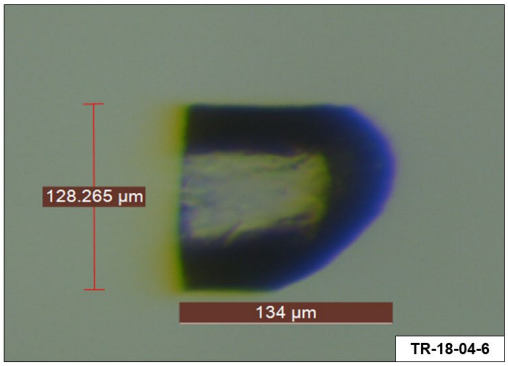
128.265 µm
134 µm
TR-18-04-6

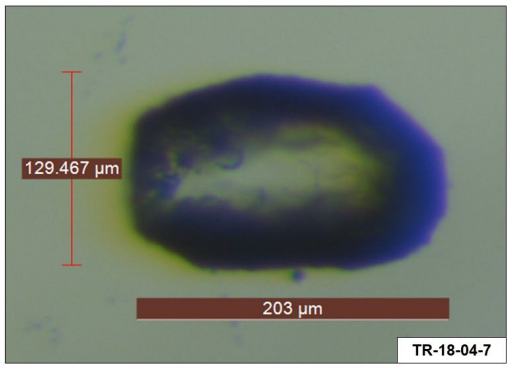
129.467 µm
203 µm
TR-18-04-7

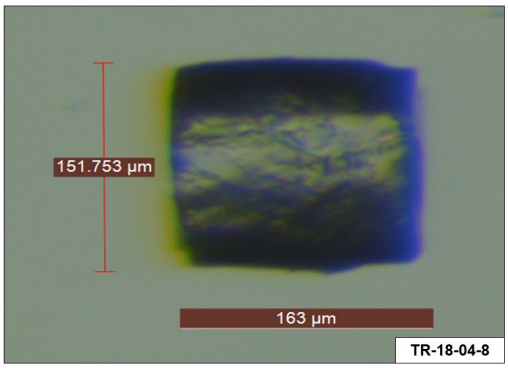
151.753 µm
163 µm
TR-18-04-8

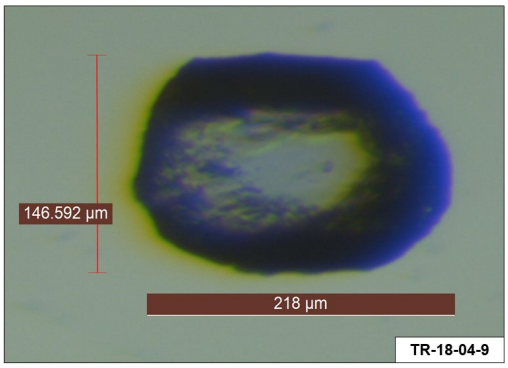
146.592 µm
218 µm
TR-18-04-9

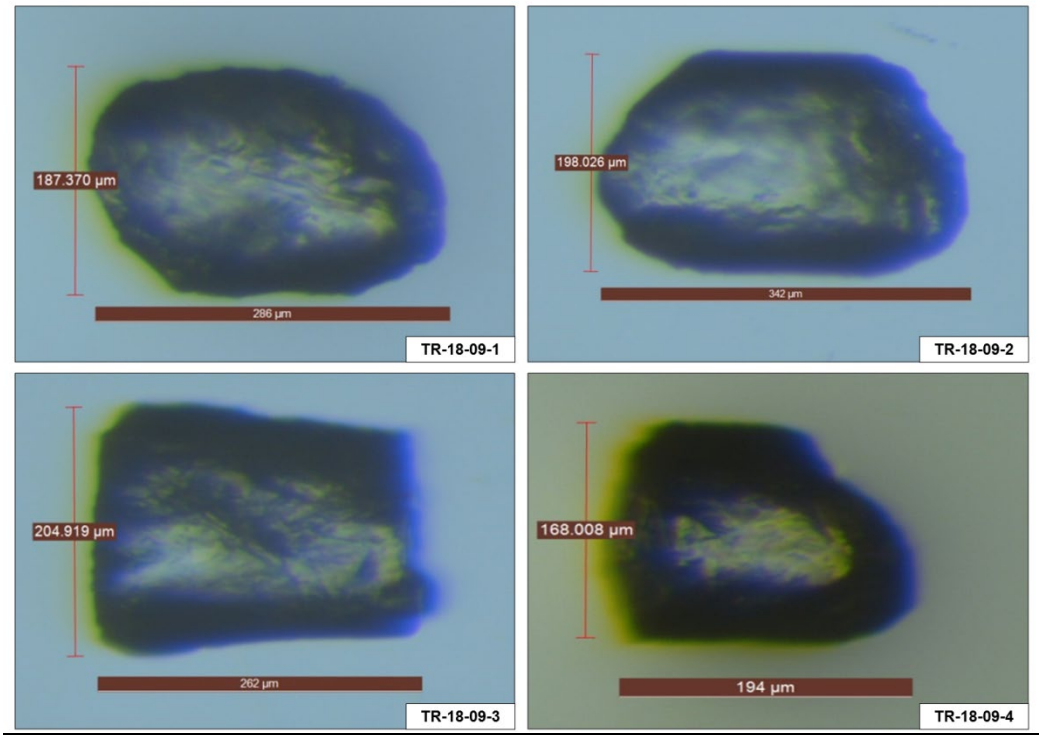
187.370 µm
286 µm
TR-18-09-1
198.026 µm
342 µm
TR-18-09-2
204.919 µm
262 µm
TR-18-09-3
168.008 µm
194 µm
TR-18-09-4

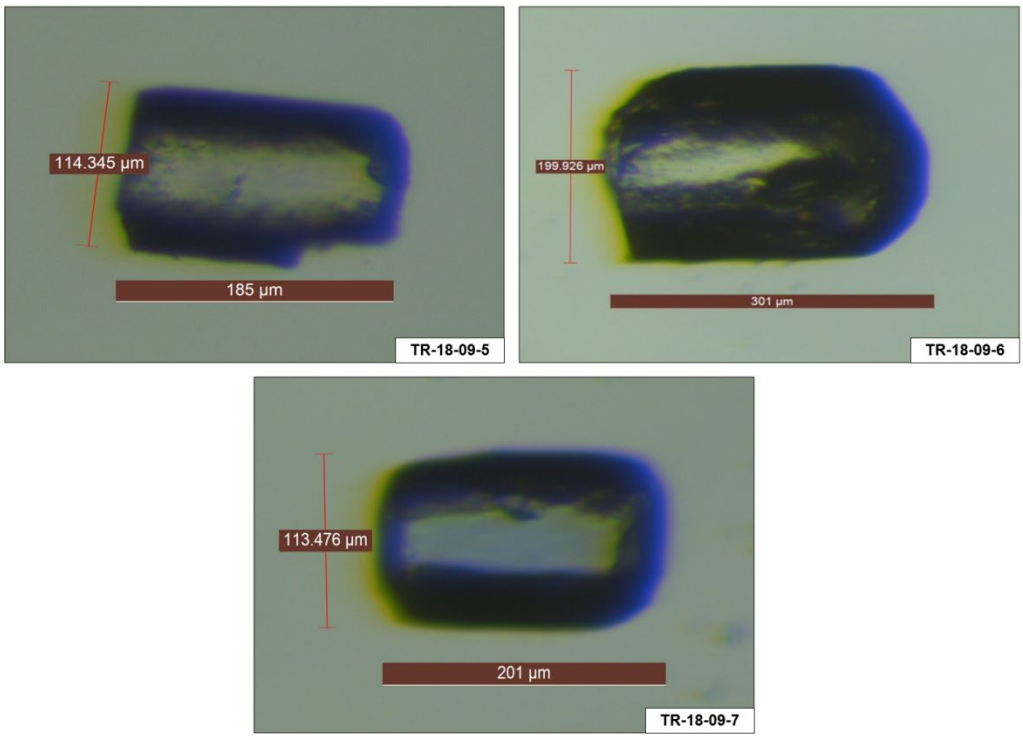
114.345 µm
185 µm
TR-18-09-5
199.926 µm
301 µm
TR-18-09-6
113.476 µm
201 µm
TR-18-09-7

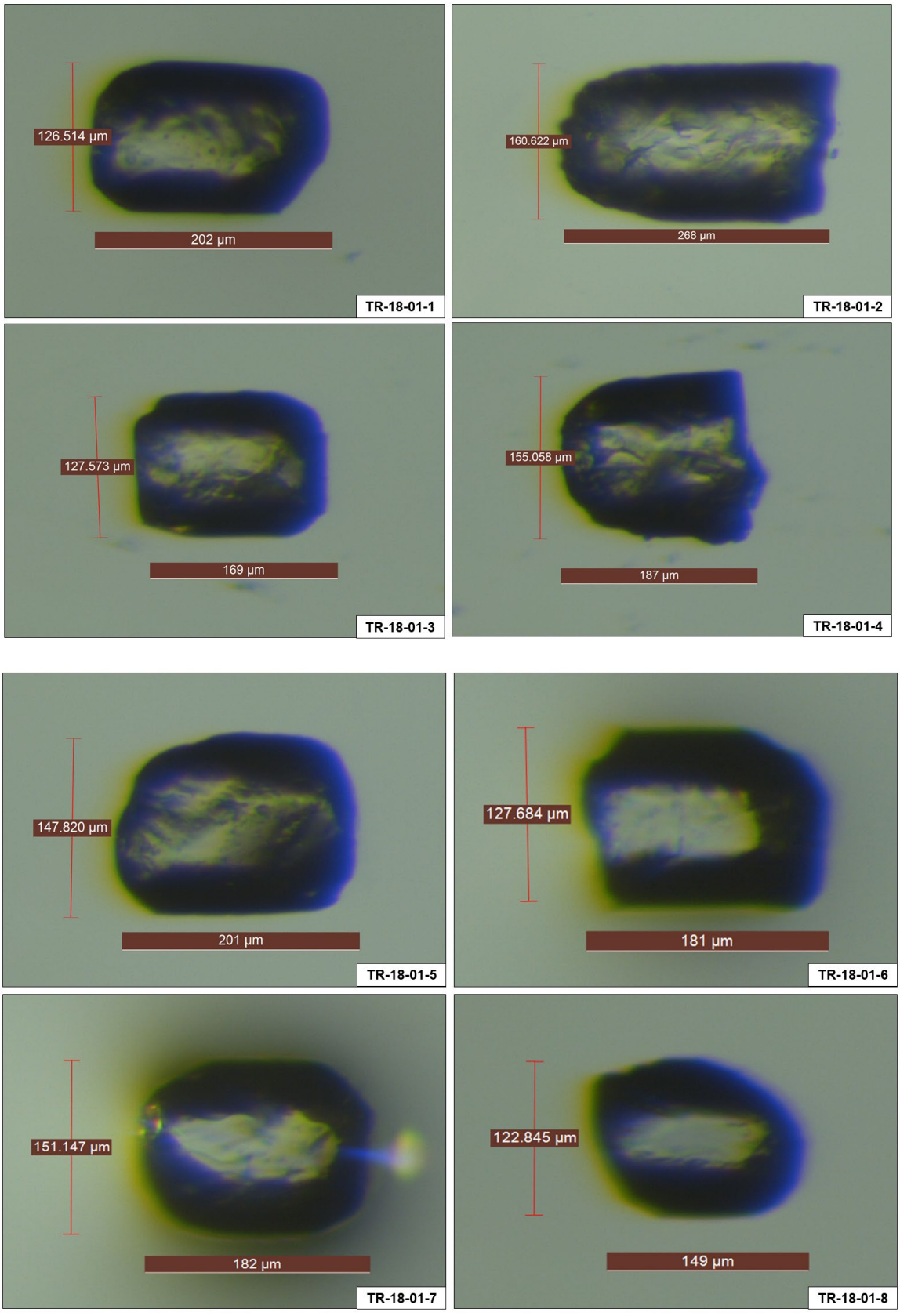
126.514 µm
202 µm
TR-18-01-1
160.622 µm
268 µm
TR-18-01-2
127.573 µm
169 µm
TR-18-01-3
155.058 µm
187 µm
TR-18-01-4
147.820 µm
201 µm
TR-18-01-5
127.684 µm
181 µm
TR-18-01-6
151.147 µm
182 µm
TR-18-01-7
122.845 µm
149 µm
TR-18-01-8

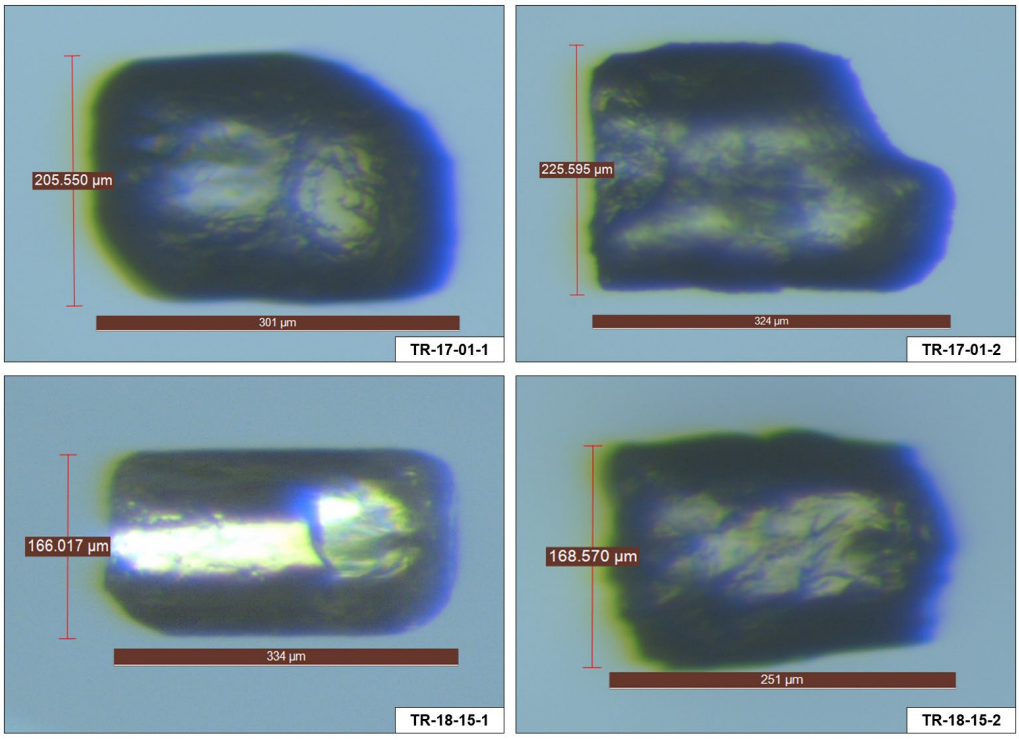
205.550 µm
301 µm
TR-17-01-1
225.595 µm
324 µm
TR-17-01-2
166.017 µm
334 µm
TR-18-15-1
168.570 µm
251 µm
TR-18-15-2

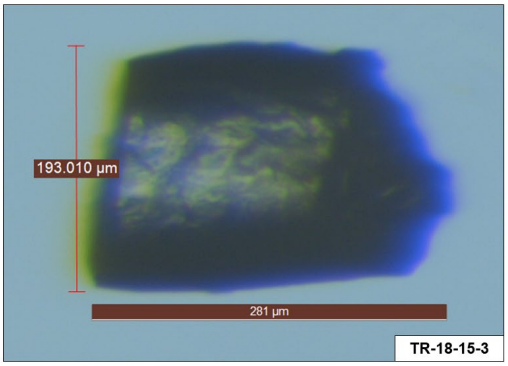
193.010 µm
281 µm
TR-18-15-3

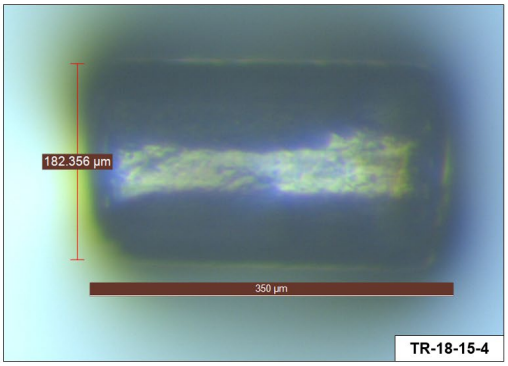
182.356 µm
350 µm
TR-18-15-4

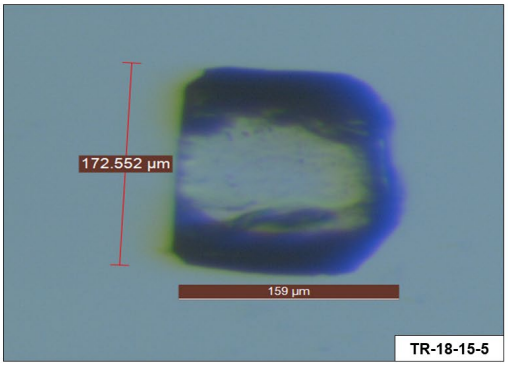
172.552 µm
159 µm
TR-18-15-5

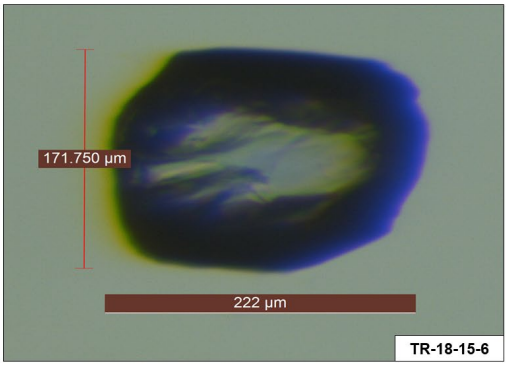
171.750 µm
222 µm
TR-18-15-6

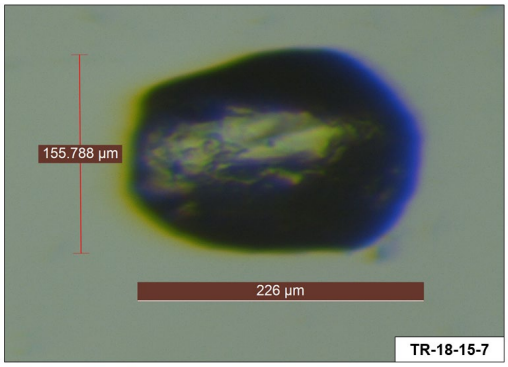
155.788 µm
226 µm
TR-18-15-7

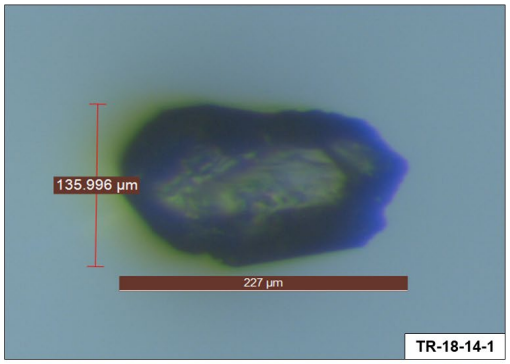
135.996 µm
227 µm
TR-18-14-1

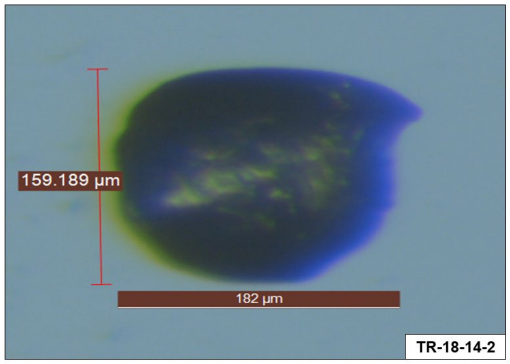
159.189 µm
182 µm
TR-18-14-2

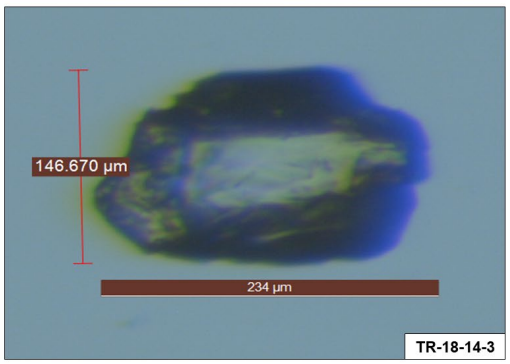
146.670 µm
234 µm
TR-18-14-3

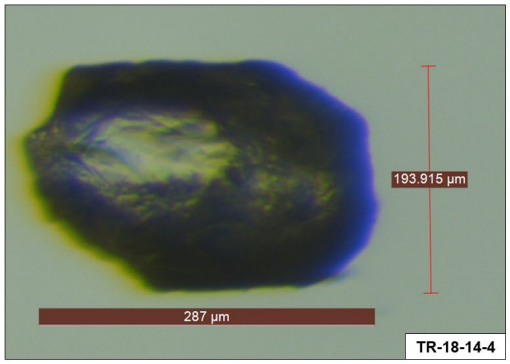
193.915 µm
287 µm
TR-18-14-4

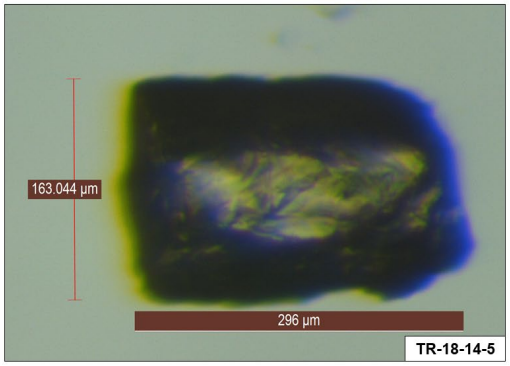
163.044 µm
296 µm
TR-18-14-5

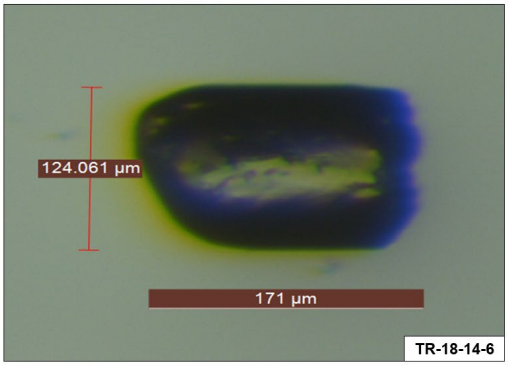
124.061 µm
171 µm
TR-18-14-6

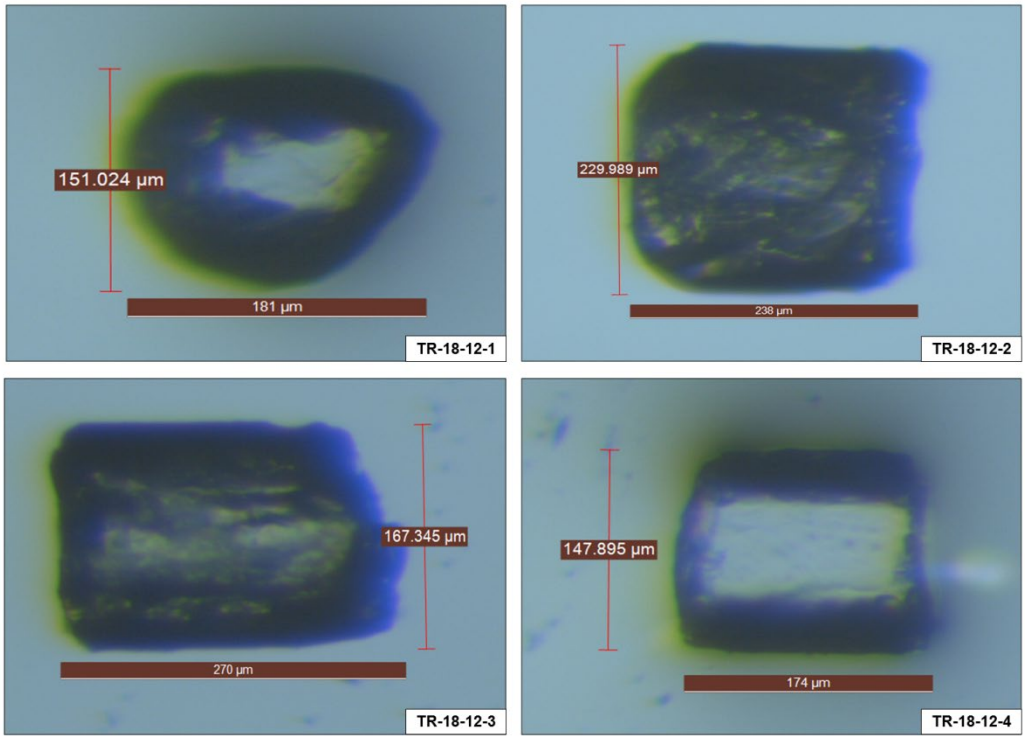
151.024 µm
181 µm
TR-18-12-1
229.989 µm
238 µm
TR-18-12-2
167.345 µm
270 µm
TR-18-12-3
147.895 µm
174 µm
TR-18-12-4

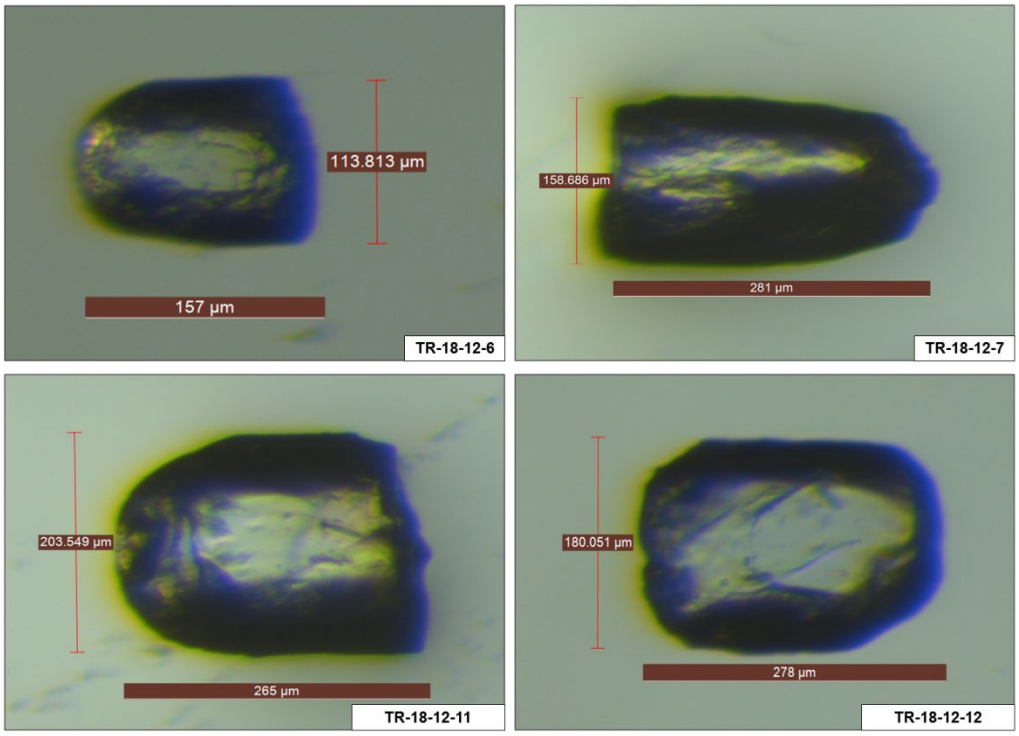
113.813 µm
157 µm
TR-18-12-6
158.686 µm
281 µm
TR-18-12-7
203.549 µm
265 µm
TR-18-12-11
180.051 µm
278 µm
TR-18-12-12

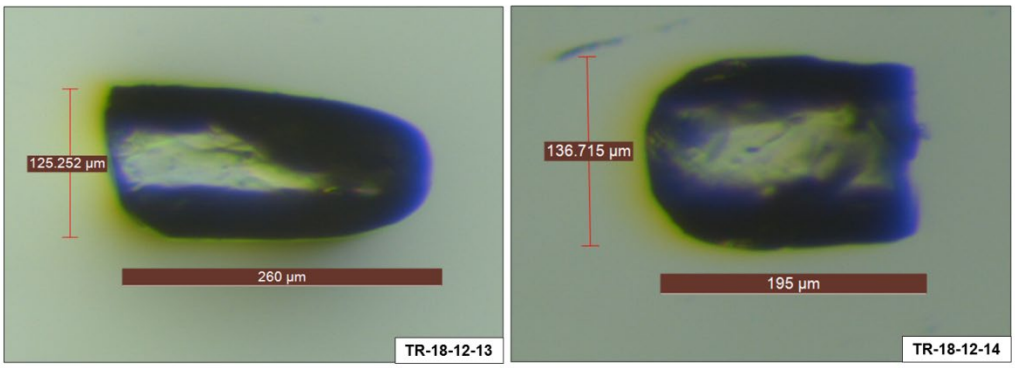
125.252 µm
260 µm
TR-18-12-13
136.715 µm
195 µm
TR-18-12-14

REFERENCES

Anders, M.H. and Sleep, N.H., 1992, Magmatism and extension: the thermal and mechanical effects of the Yellowstone hotspot: Journal of Geophysical Research v. 97 (B11), p. 15379-15393.

Braun, J., 2005, Quantitative constraints on the rate of landform evolution from low temperature thermochronology, in Reiners, P.W. and Ehlers, T.A. eds., Low temperature thermochronology: Techniques, Interpretations, and Applications: Mineralogical Society of America Reviews in Mineralogy and Geochemistry, v. 58, p. 351-374.

Brown, S. J., Thigpen, J. R., Spotila, J. A., Krugh, W. C., Tranel, L. M., & Orme, D. A. (2017). Onset timing and slip history of the Teton fault, Wyoming: A multidisciplinary reevaluation. Tectonics, 36. p. 1-24.

Byrd, J.O.D., Smith, R.B., and Geissman, J.W., 1994, The Teton fault, Wyoming: Topographic signature, neotectonics, and mechanisms of deformation: Journal of Geophysical Research, v. 99, p. 20095–20122.

Dadson, S. J. et al., 2003, Links between erosion, runoff variability and seismicity in the Taiwan orogen. Nature 426, 448–451.

Densmore, A.L., Dawers, N.H., Gupta, S., and Guidon, R., 2005, What sets topographic relief in extensional foot-walls?: Geology, v. 33, no. 6, p. 453–456.

Ehlers, T.A., Armstrong, P.A., Chapman, D.S., 2001, Normal fault thermal regimes and the interpretation of low-temperature thermochronometers: Physics of the Earth and Planetary Interiors, v. 126, p. 179–194.

Ehlers, T.A., Farley, K.A., 2003, Apatite (U-Th)/He thermochronometry; methods and applications to problems in tectonic and surface processes: Earth and Planetary

Science Letters, v. 206, no. 1–2, p. 1–14.

Ehlers, T. A., 2005, Crustal thermal processes and the interpretation of thermochronometer data, in Reiners, P. W., and Ehlers, T. A., eds., LowTemperature Thermochronology: Techniques, Interpretations, and Applications, Volume 58: Chantilly, VA, Mineralogical Society of America, p. 315-350.

Ellis, M.A., Densmore, A.L., Anderson, R.S., 1999, Development of mountainous topography in the Basin and Ranges, USA: Basin Research, v. 11, no. 1, p. 21–41. 53

England, P., and Molnar, P., 1990, Surface uplift, uplift of rocks, and exhumation of rocks: Geology, v. 18, no. 12, p. 1173– 1177.

Farley, K.A., 2002, (U-Th)/He dating: Techniques, calibrations, and applications, in Portcelli, D., Ballentine, C.J., and Wieler, R., eds., Noble Gases in Geochemistry and Cosmochemistry, Volume 47: Washington, D.C., Mineralogical Society of America, p. 819–843.

Farley, K.A. and Stockli, D.F., 2002, (U-Th)/He dating of phosphates; apatite, monazite, and xenotime, in Kohn, M.J.R., John; Hughes, John M, ed., Reviews in Mineralogy and Geochemistry, Volume 48: Washington, DC, Mineralogical Society of America and Geochemical Society, p. 559-577.

Foster, D., Brocklehurst, S.H., and Gawthorpe, R.L., 2008, Small valley glaciers and the effectiveness of the glacial buzzsaw in the northern Basin and Range, USA: Geomorphology, v. 102, p. 624–639, doi: 10.1016/j.geomorph.2008.06.009.

Foster, D., Brocklehurst, S.H., and Gawthorpe, R.L., 2010, Glacial-topographic interactions in the Teton Range, Wyoming: Journal of Geophysical Research, v. 115, p. 1–20.

Gallagher, K., 2012, Transdimensional inverse thermal history modeling for quantitative thermochronology: Journal of Geophysical Research, v. 117, p. 1-16.

Godard, V., Lavé, J., and Cattin, R., 2006, Numerical modelling of erosion processes in the Himalayas of Nepal: effects of spatial variations of rock strength and precipitation: Geological Society, London, Special Publications, v. 253, p. 341–358, doi: 10.1144/gsl.sp.2006.253.01.18.

Godard, V., Bourles, D.L., Spinabella, F., Burbank, D.W., Bookhagen, B., Fisher, G.B., Moulin, A., and Leanni, L., 2014, Dominance of tectonics over climate in Himalayan denudation: Geology, v. 42, p. 243–246, doi: 10.1130/g35342.1.

Hampel, A., Hetzel, R., Densmore, A.L., 2007, Postglacial slip-rate increase on the Teton normal fault, northern Basin and Range Province, caused by melting of the Yellowstone ice cap and deglaciation of the Teton Range?: Geology, v. 35, no. 12, p. 1107.

Harrison, T.M., Zeitler, P.K., 2005, Fundamentals of noble gas thermochronometry. Reviews in Mineralology and Geochememistry, v. 58, p. 123-149.

Hoar, R., Thigpen, J., & University of Kentucky. College of Arts Sciences, degree granting institution. (2018). Refining the onset timing and slip history along the northern part of the Teton fault.

Ketcham, R.A., 2005, Forward and inverse modeling of low-temperature thermochronometry data, in Reiners, P.W. and Ehlers, T.A. eds., Lowtemperature thermochronology: Techniques, Interpretations, and Applications: Mineralogical Society of America Reviews in Mineralogy and Geochemistry, v. 58, p. 275-314, doi:10.2138/rmg.2005.58.11.

Kindinger, J.G., Davis, J.B., and Flocks, J.G., 1994, High-resolution single-channel seismic reflection surveys of Orange Lake and other selected sites of north central Florida: Open-File Report, doi: 10.3133/ofr94616.

Konstantinovskaia, E., and Malavieille, J., 2005, Erosion and exhumation in accretionary orogens: Experimental and geological approaches: Geochemistry, Geophysics, Geosystems, v. 6, doi: 10.1029/2004gc000794.

Koppes, M.N., and Montgomery, D.R., 2009, The relative efficacy of fluvial and glacial erosion over modern to orogenic timescales: Nature Geoscience, v. 2, p. 644–647, doi: 10.1038/ngeo616.

Lageson, D.R., Adams, D.C., Morgan, L.A., Pierce, K.L., and Smith, R.B., 1999, Neogene-Quaternary Tectonics and Volcanism of southern Jackson Hole, Wyoming and southeastern Idaho, in Hughes, S.S., Thackray, G.D., eds., Guidebook to the Geology of Eastern Idaho: Pocatello, Idaho Museum of Natural History, p. 115-130.

Larsen, et. al, 2016, Deglaciation and postglacial environmental changes in the Teton Mountain Range recorded at Jenny Lake, Grand Teton National Park, WY: Quaternary Science Reviews, v. 138, p. 62-73.

Leopold, E. B., Liu, G., Love, J. D., Love, D. W., 2007, Plio-Pleistocene climatic transition and the lifting of the Teton Range, Wyoming, Quaternary Research, 67, 1- 11.

Love, J. D., Reed, J. C., and Pierce, K. L., 2003, Creation of the Teton landscape; a geologic chronicle of Jackson hole and the Teton range: Grand Teton Natural History Association, 2nd ed.

Milliman, J.D., and Syvitski, J.P.M., 1992, Geomorphic/Tectonic Control of Sediment Discharge to the Ocean: The Importance of Small Mountainous Rivers: The Journal of Geology, v. 100, p. 525–544, doi: 10.1086/629606.

Peyton, S.L. and Carrapa, B., 2013, An introduction to low-temperature thermochronologic techniques, methodology, and applications, in C. Knight and J. Cuzella, eds., Application of structural methods to Rocky Mountain hydrocarbon exploration and development: AAPG Studies in Geology 65, p. 15–36.

Pierce, K.L., and Licciardi, J.M., 2018, History and dynamics of the Greater Yellowstone Glacial System during the last two glaciations: Quaternary Science Reviews, v. 200, p. 1–33, doi: 10.1016/j.quascirev.2018.08.027.

Pierce, K.L., and Morgan, L.A., 2009, Is the track of the Yellowstone Hot Spot driven by a deep mantle plume? Review of volcanism, faulting, and uplift in light of new data: Journal of Volcanology and Geothermal Research, v. 188, no. 1-3, p. 1-25.

Scholz, C. H., 2002, The Mechanics of Earthquakes and Faulting, 2nd Ed. Cambridge: Cambridge University Press.

Reed, J.C., and Zartman, R.E., 1973, Geochronology of Precambrian Rocks of the Teton Range, Wyoming: Geological Society of America Bulletin, v. 84, p. 561, doi: 10.1130/0016-7606(1973)84<561:goprot>2.0.co;2.

Roberts, S.V., and Burbank, D.W., 1993, Uplift and thermal history of the Teton Range (northwestern Wyoming) defined by apatite fission-track dating: Earth and Planetary Science Letters, v. 118, p. 295–309.

Roe, G.H., and Brandon, M.T., 2011, Critical form and feedbacks in mountain-belt dynamics: Role of rheology as a tectonic governor: Journal of Geophysical Research, v. 116, doi: 10.1029/2009jb006571.

Spotila, J. A., 2005, Applications of Low-Temperature Thermochronometry to Quantification of Recent Exhumation in Mountain Belts: Reviews in Mineralogy and Geochemistry, v. 58, no. 1, p. 449-466. 58

Stockli, D.F., 2005, Application of low-temperature thermochronometry to extensional tectonic settings, in Reiners, P.W., and Ehlers, T.A., eds., Low-Temperature Thermochronology: Techniques, Interpretations, & Applications: Mineralogical Society of America, Reviews in Mineralogy and Geochemistry Volume 58, p. 411–448 and references therein.

Thackray, Glenn D., and Staley, Amie E., 2017, Systematic variation of Late Pleistocene fault scarp height in the Teton Range, Wyoming, USA: Variable fault slip rates or variable landform ages?: Geosphere, v. 13, no. 2, p. 287-300, doi: 10.1130/GES01320.1.

Tranel, L.M., Spotila, J.A., Kowalewski, M.J., and Waller, C.M., 2011, Spatial variation of erosion in a small, glaciated basin in the Teton Range, Wyoming, based on detrital apatite (U-Th)/He thermochronology: Basin Research, v. 23, p. 571–590, doi: 10.1111/j.1365-2117.2011.00502.x.

Tranel, L.M., and Strow, M.L., 2017, 10Be analysis of amalgamated talus pebbles to investigate alpine erosion, Garnet Canyon, Teton Range, Wyoming: Geosphere, v. 13, no. 1, doi: 10.1130/GES01297.1.

Twichell, D.C., Cross, V.A., Hanson, A.D., Buck, B.J., Zybala, J.G., & Rudin, M.J., 2005. Seismic architecture and lithofacies of turbidites in Lake Mead (Arizona and

Nevada, U.S.A.), an analogue for topographically complex basins: Journal of Sedimentary Research, v. 75, no. 1, p 134-148. https://doi.org/10.2110/jsr.2005.011

Tyagi, A.K., et al., 2009. Identifying areas of differential uplift using steepness index in the Alaknanda basin, Garhwal Himalaya, Uttarakhand: Current Science, v. 97, no. 10, p. 1473-1477.

Whipple, K., and Meade, B., 2006, Orogen response to changes in climatic and tectonic forcing: Earth and Planetary Science Letters, v. 243, p. 218–228, doi: 10.1016/j.epsl.2005.12.022.

Whipple, K.X., 2009, The influence of climate on the tectonic evolution of mountain belts: Nature Geoscience, v. 2, p. 97–104, doi: 10.1038/ngeo413.

White, B.J.P., Smith, R.B., Husen, S., Farrell, J.M., and Wong, I., 2009, Seismicity and earthquake hazard analysis of the Teton-Yellowstone region, Wyoming: Journal of Volcanology and Geothermal Research, v. 188, p. 277-296.

Whittaker, Alexander C., 2012, How do landscapes record tectonics and climate?: Lithosphere, v. 4, p. 160-164.

Willett, S.D., 1999, Orogeny and orography: The effects of erosion on the structure of mountain belts: Journal of Geophysical Research: Solid Earth, v. 104, p. 28957–28981, doi: 10.1029/1999jb900248.

Zeitler, P.K., Herczeg, A.L., McDougall, I., and Honda, M., 1987, U-Th-He dating of apatite: a potential thermochronometer: Geochima et Cosmochimica Acta, v. 51, p. 2865 – 2868.

VITA

Meredith Leigh Swallom

Education

B.S. Geological Sciences (2017)

University of Kentucky

Experience

Graduate Teaching/Research Assistant

Structure and Geodynamics Lab

Department of Earth and Environmental Sciences

University of Kentucky, 40506

Undergraduate Research Assistant

Pioneer Paleoenvironments and Stratigraphy Lab

Department of Earth and Environmental Sciences

University of Kentucky, 40506